

Nuclear structure: part 2

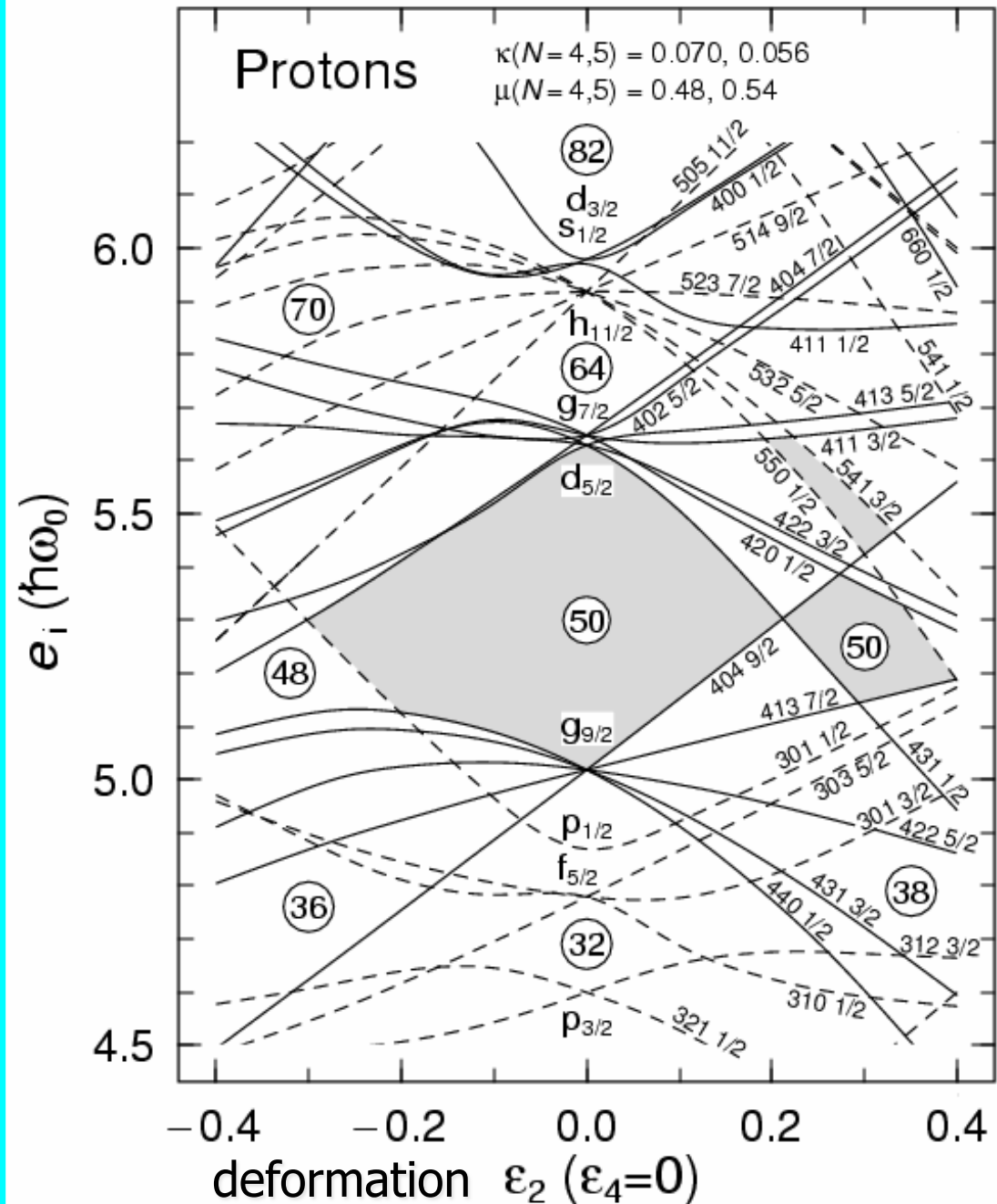
Anatoli Afanasjev
Mississippi State University

1. Nuclear theory – selection of starting point
2. What can be done 'exactly' (*ab-initio* calculations) and why we cannot do that systematically?
3. Effective interactions
4. Density functional theory
5. Shell structure and shell effects. Their consequences.
6. Nuclear landscape: what we know and how well we extrapolate
7. Superheavy nuclei
8. Going beyond mean field approximation: particle-vibration coupling in spherical nuclei
9. Rotation in nuclei

Reminder from previous lecture

Deformation dependence of the single-particle energies in a realistic Nilsson potential

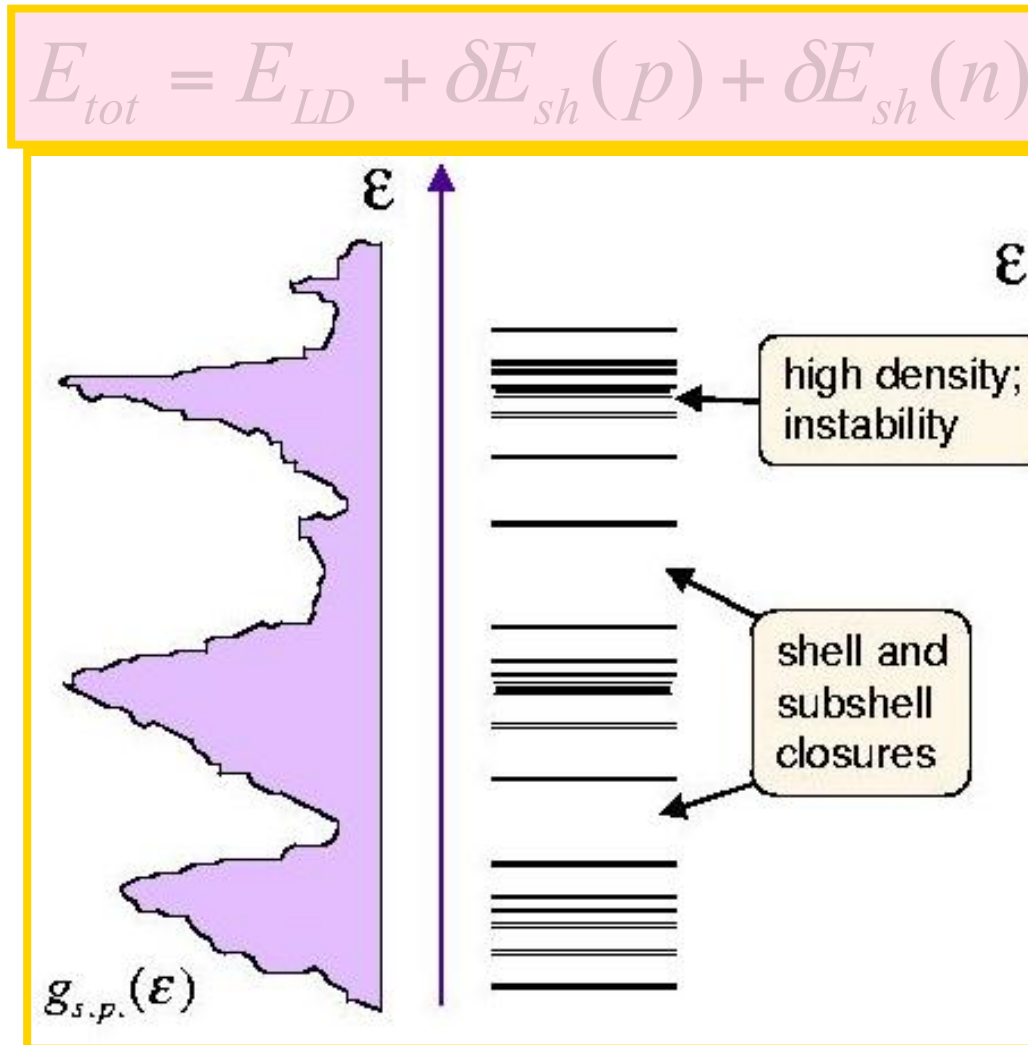
1. removing of the $2j+1$ degeneracy of single-particle state seen at spherical shape
2. single-particle states at deformation ε_2 not equal 0 are only two-fold degenerate
3. creation of deformed shell gaps



Shell structure and shell correction energies

$$\delta E_{shell} = 2 \sum_{\nu} e_{\nu} - 2 \int e \tilde{g}(e) de \quad \text{shell correction energy}$$

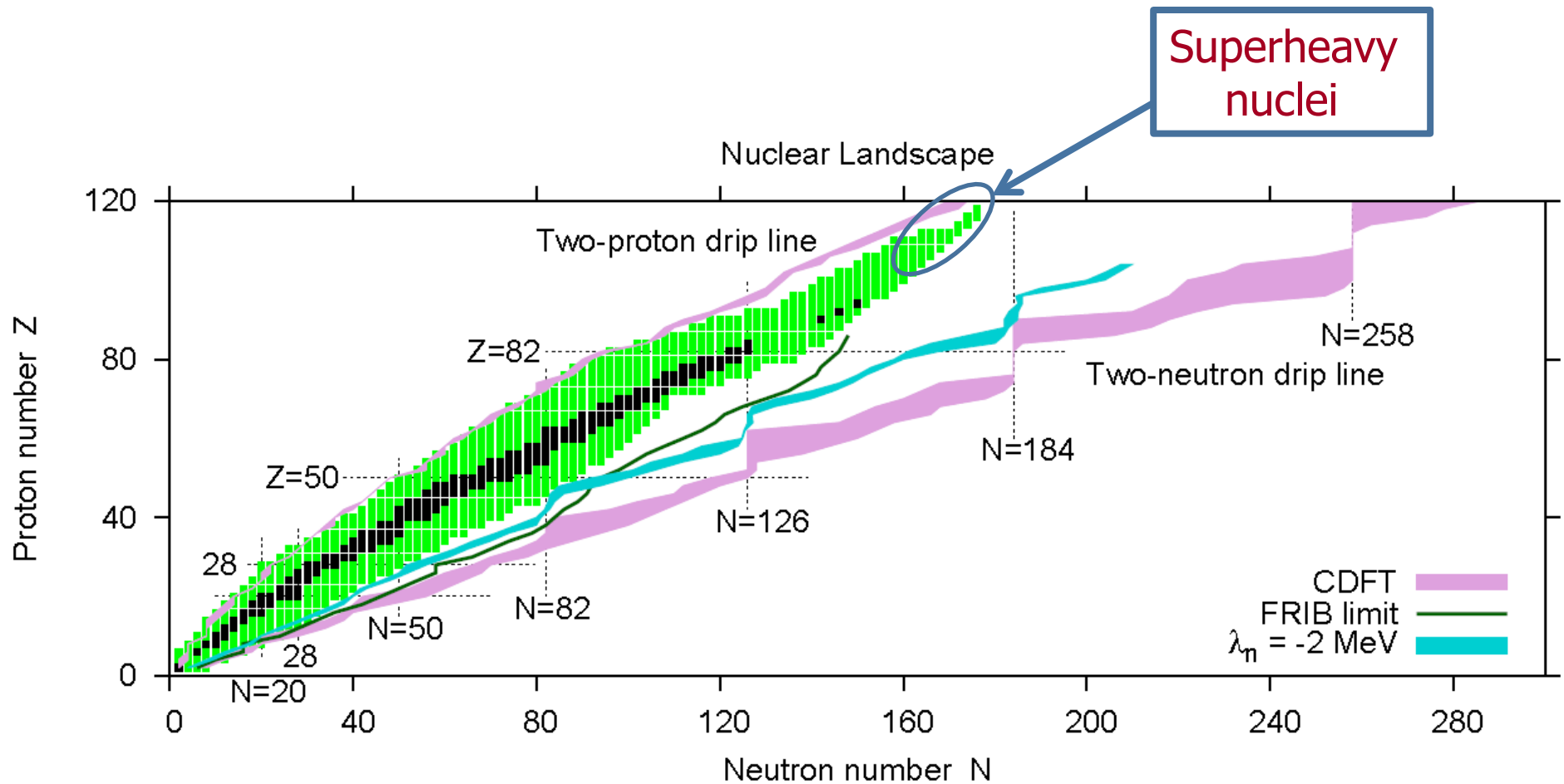
e_{ν} - single-particle energies $\tilde{g}(e)$ - smeared level density



$$\delta E_{shell} > 0$$

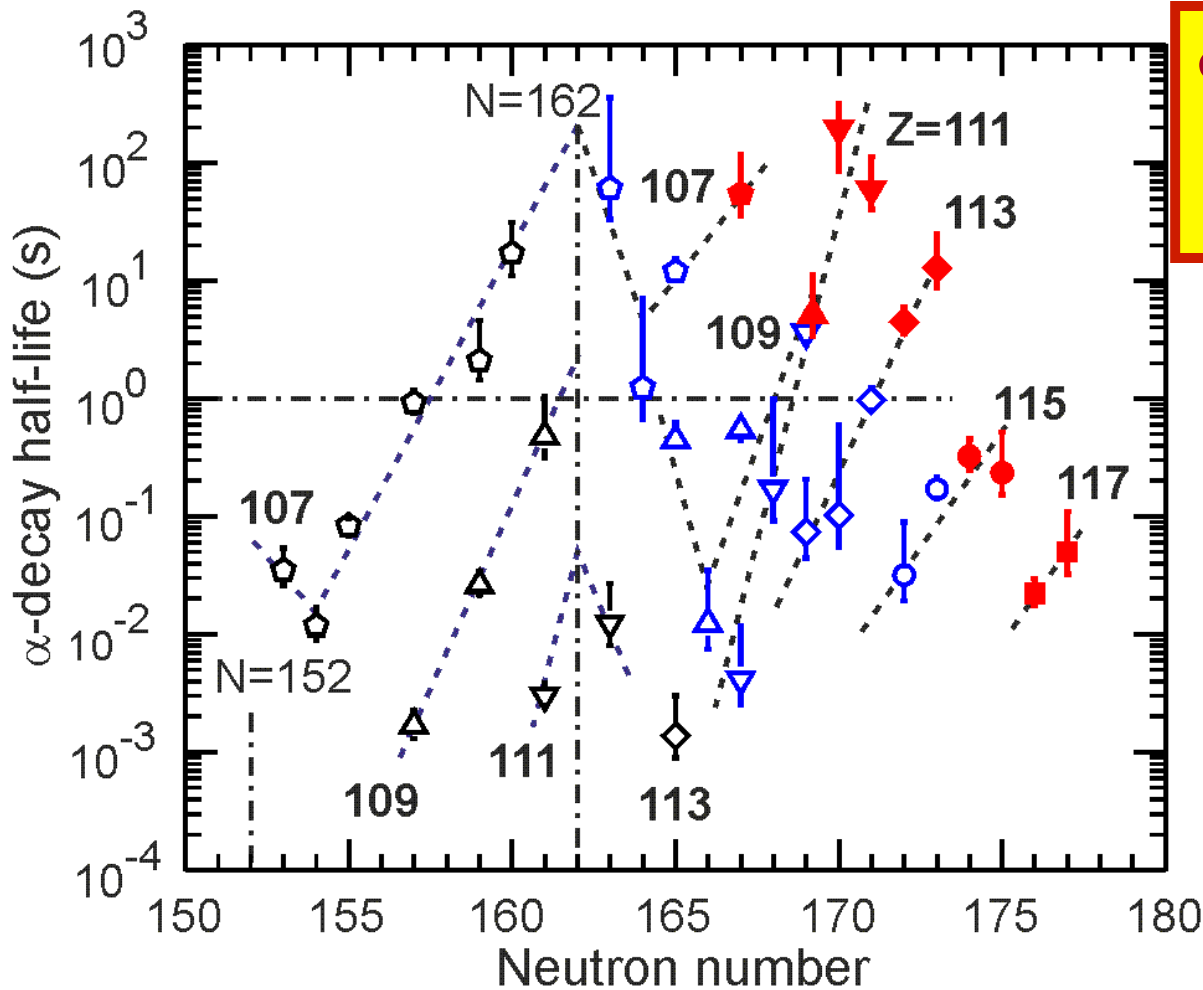
$$\delta E_{shell} < 0$$

Superheavy nuclei



Stability of superheavy nuclei is determined exclusively by quantum (shell) effects

Competition of two processes after formation of superheavy nucleus: spontaneous fission and α -decay

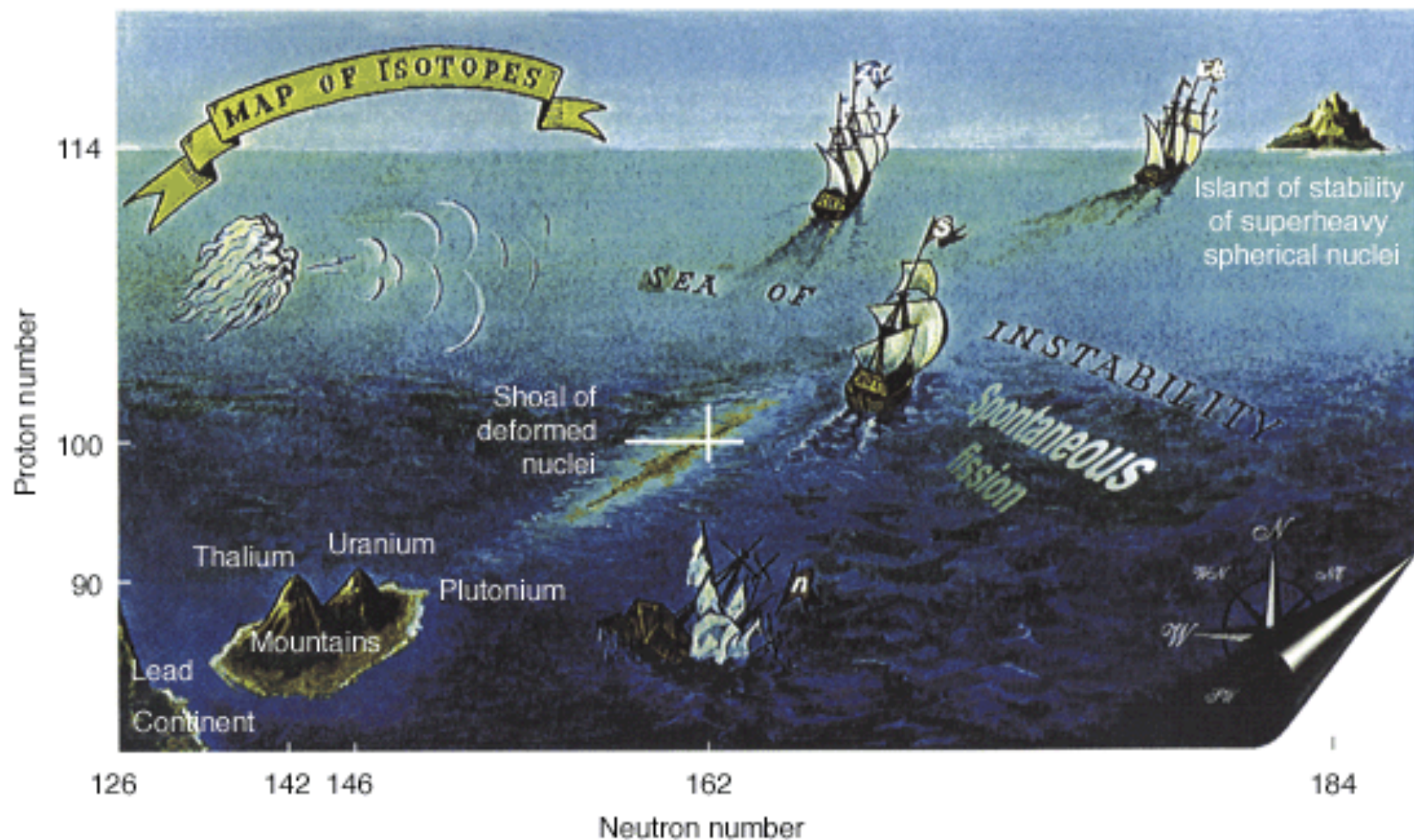


α -decay half-life times:
indication of the island
of enhanced stability

Viola-Seaborg formula

$$\log_{10} T_{\alpha} = (aZ + b) Q_{\alpha}^{-1/2} + (cZ + d)$$

1. Increase of stability on approaching deformed N=162 shell gap
2. Increase of stability on increase of N above 166



A Russian artist depicts the modern nuclear theory of the heaviest elements. At the upper far right is the island of stability, which was demonstrated by the production of long-lived element 114 in 1998 by a Russian–Livermore team.

Physics of superheavy nuclei

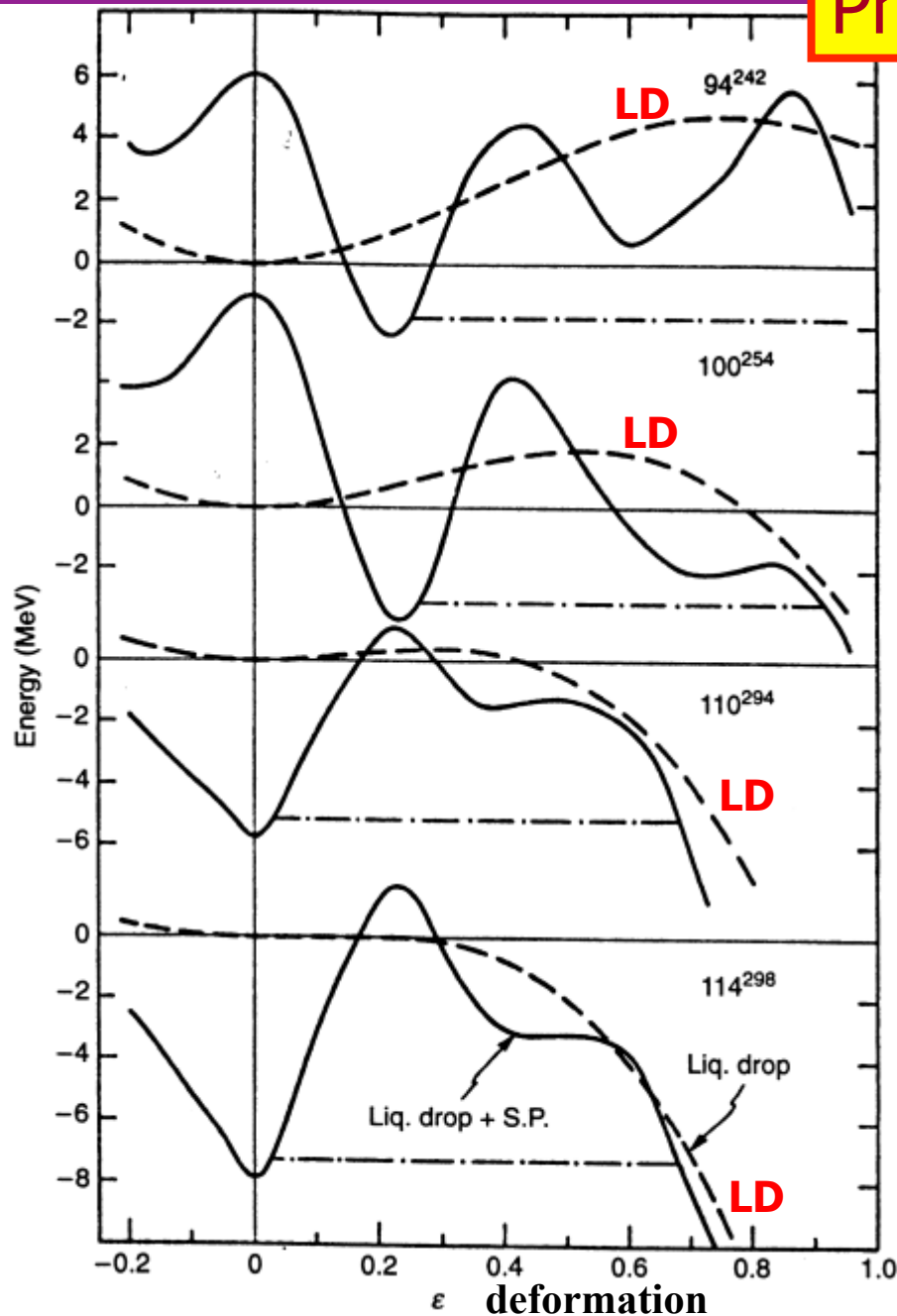
Macroscopic + microscopic approach

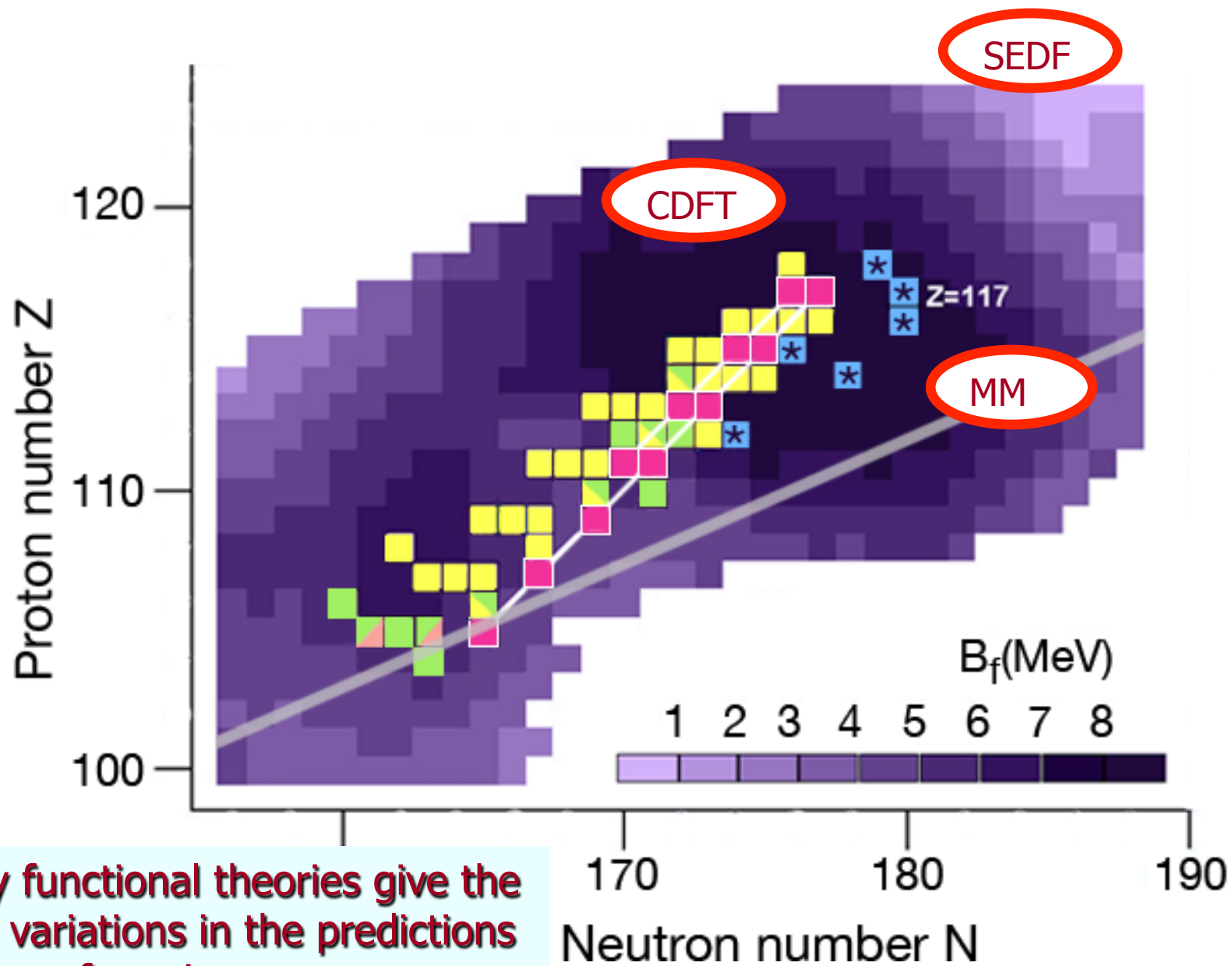
$$E_{tot} = E_{LD} + \delta E_{shell} + E_{pair}$$

liquid drop
 quantum (shell) correction
 pairing

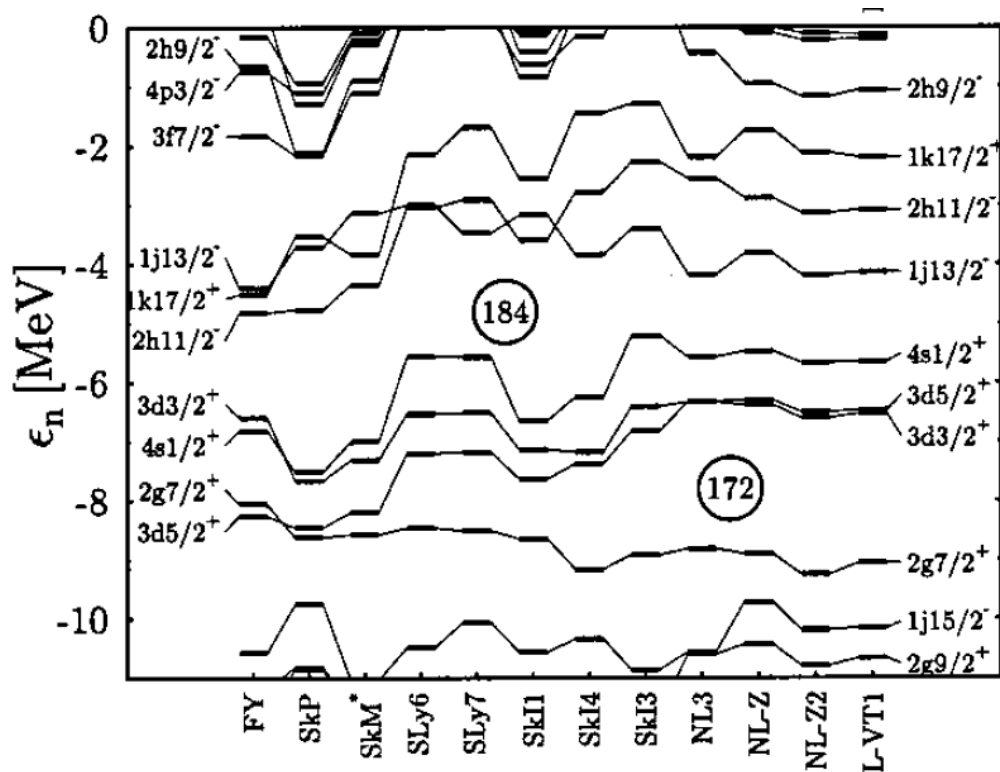
Liquid-drop fission barrier vanishes

**Stability of superheavy nuclei
 is determined exclusively by
 quantum (shell) effects**

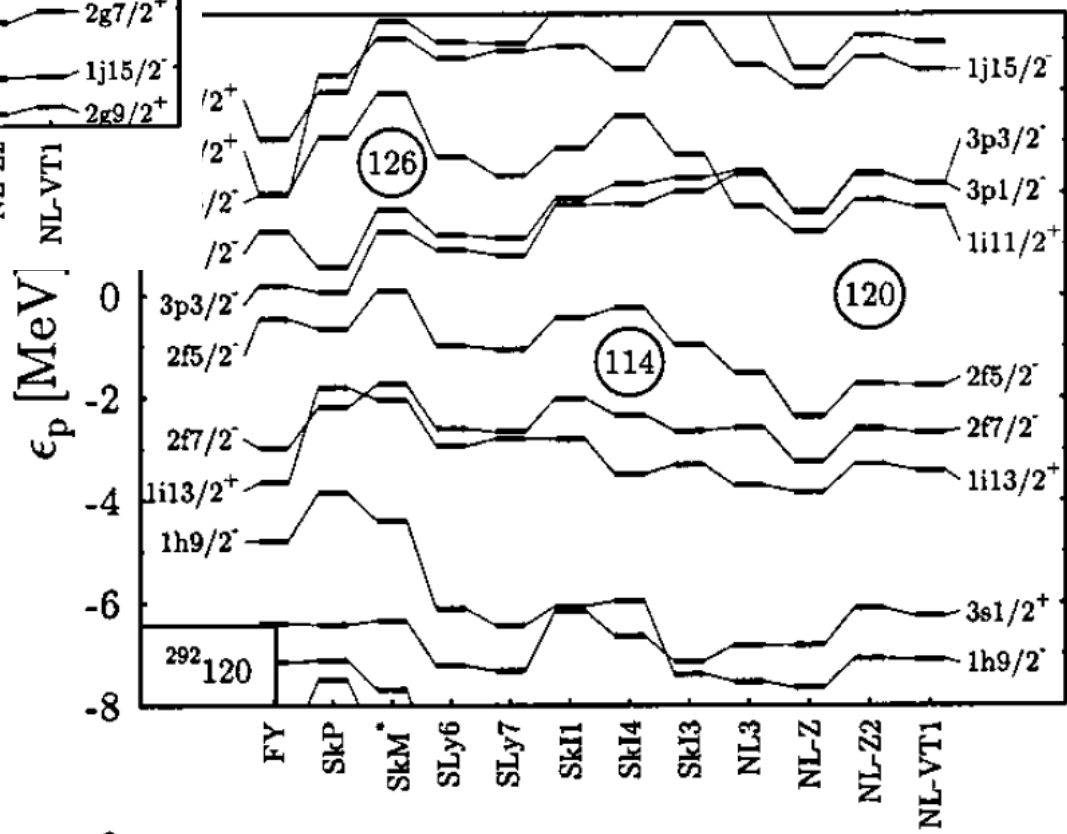




Density functional theories give the largest variations in the predictions of magic gaps at $Z=120, 126$ and $172, 184$

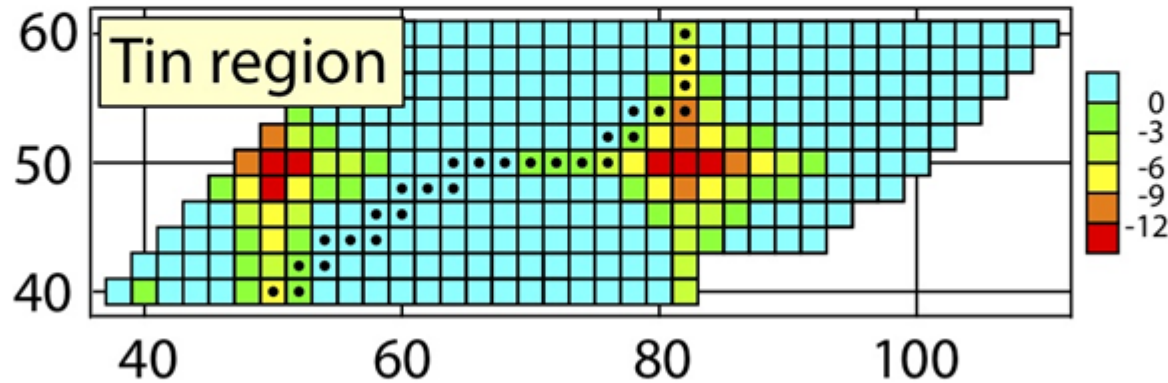


Shell structure and shell gaps in spherical superheavy nuclei

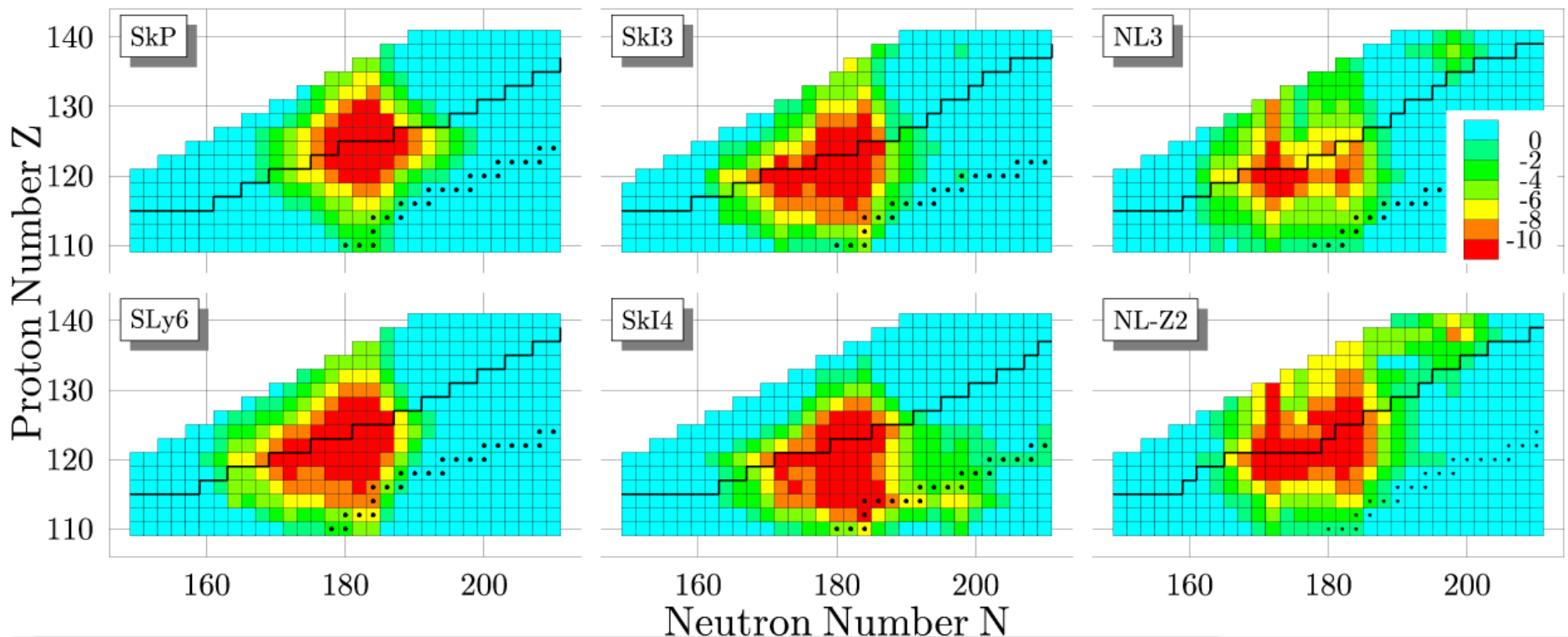


Bender et al, PRC 60, 034304 (1999)

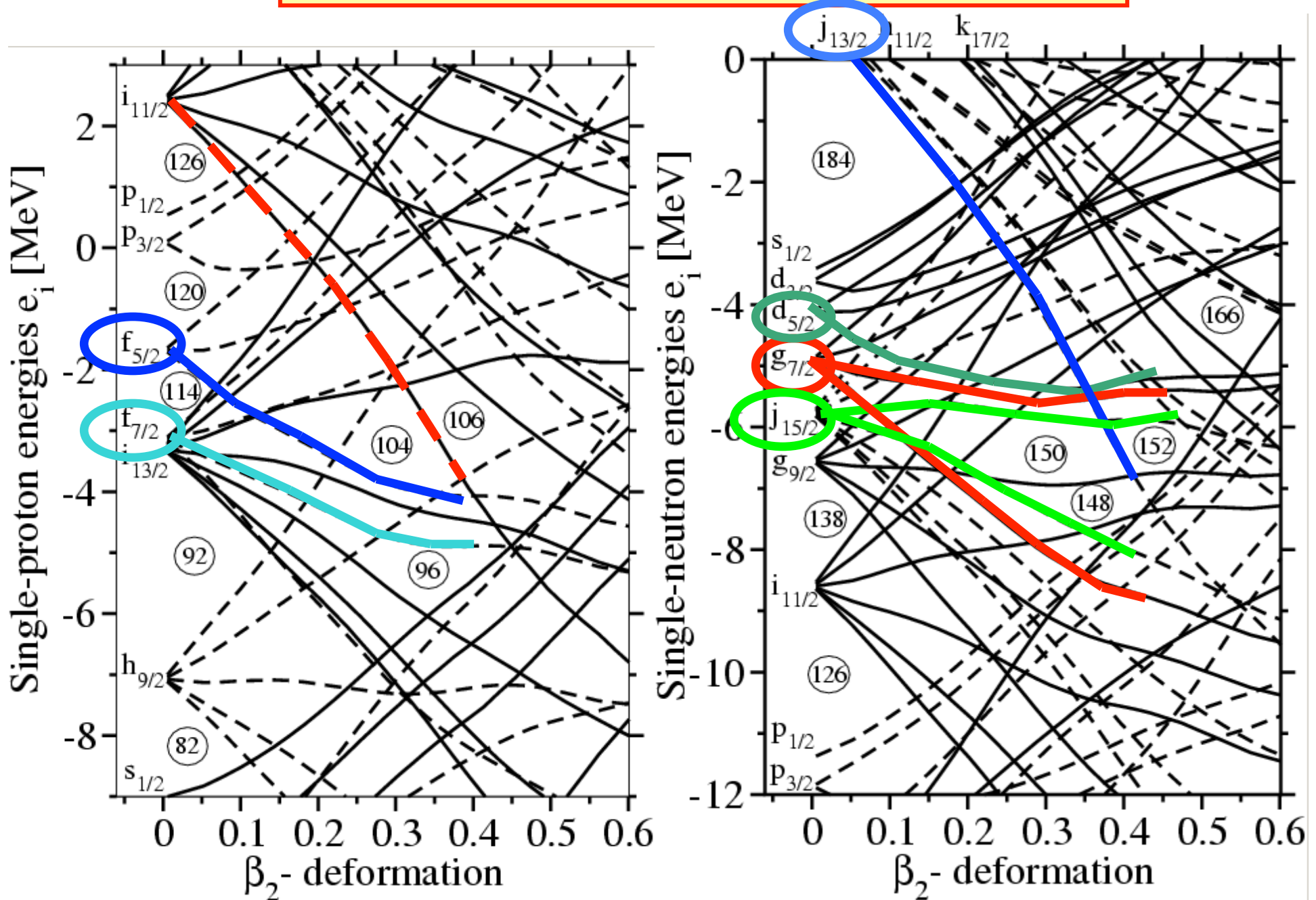
Shell correction energy: difference between tin and SHE regions



M.Bender, W.Nazarewicz,
P.-G.Reinhard,
PLB 515, 42 (2001)



CDFT calculations for ^{252}No with the NL1 functional



What are the possible sources of different centers of the islands of SHE?

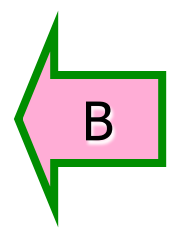
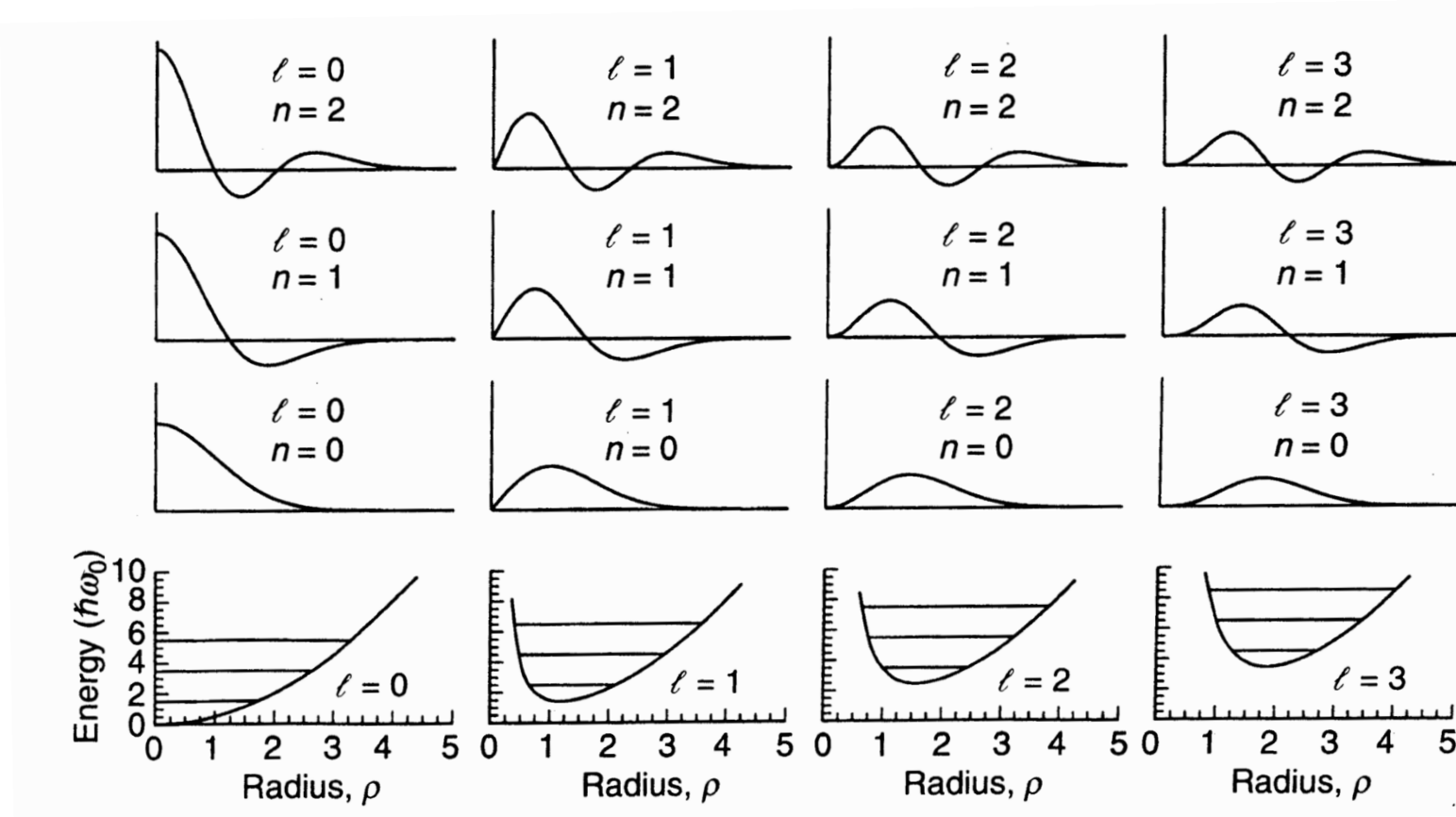
- **self-consistency effects [density profiles]**

may explain mic+mac vs DFT

- **spin-orbit splittings**

may explain CDFT versus Skyrme DFT

Lesson from quantum mechanics: spherical harmonic oscillator

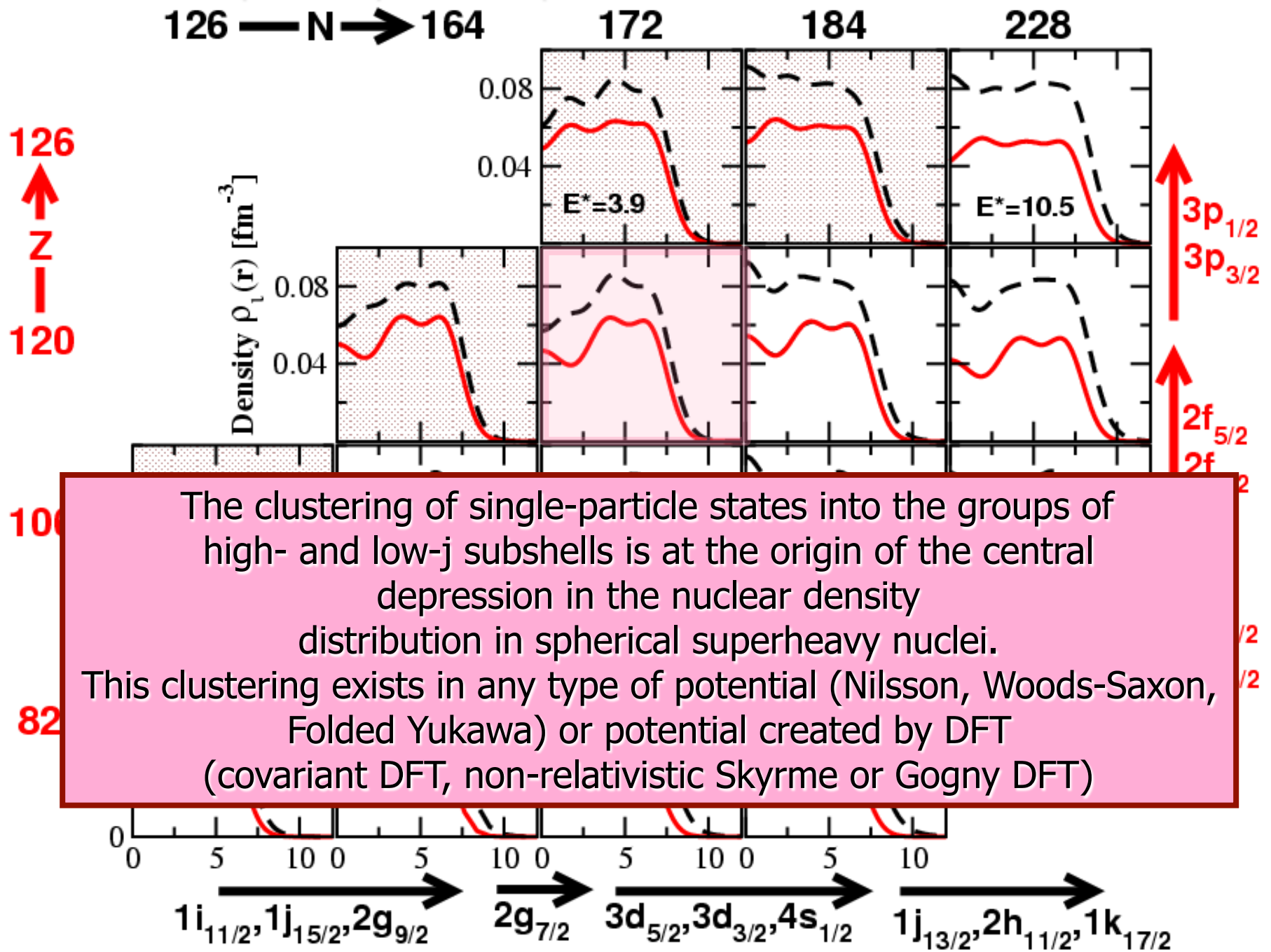


A: the radial wave function $R(\rho)$

B: effective radial potential, i.e. with the centrifugal term

$$\frac{\hbar^2 l(l+1)}{2Mr^2} \quad \text{added.}$$

Densities of superheavy nuclei: spherical CDFT calculations with the NL3 force



The clustering of single-particle states into the groups of high- and low- j subshells is at the origin of the central depression in the nuclear density distribution in spherical superheavy nuclei. This clustering exists in any type of potential (Nilsson, Woods-Saxon, Folded Yukawa) or potential created by DFT (covariant DFT, non-relativistic Skyrme or Gogny DFT)

Skyrme SkP [$m^*/m=1$]
**double shell closure
 at $Z=126, N=184$**
 (SkM*, **????**)

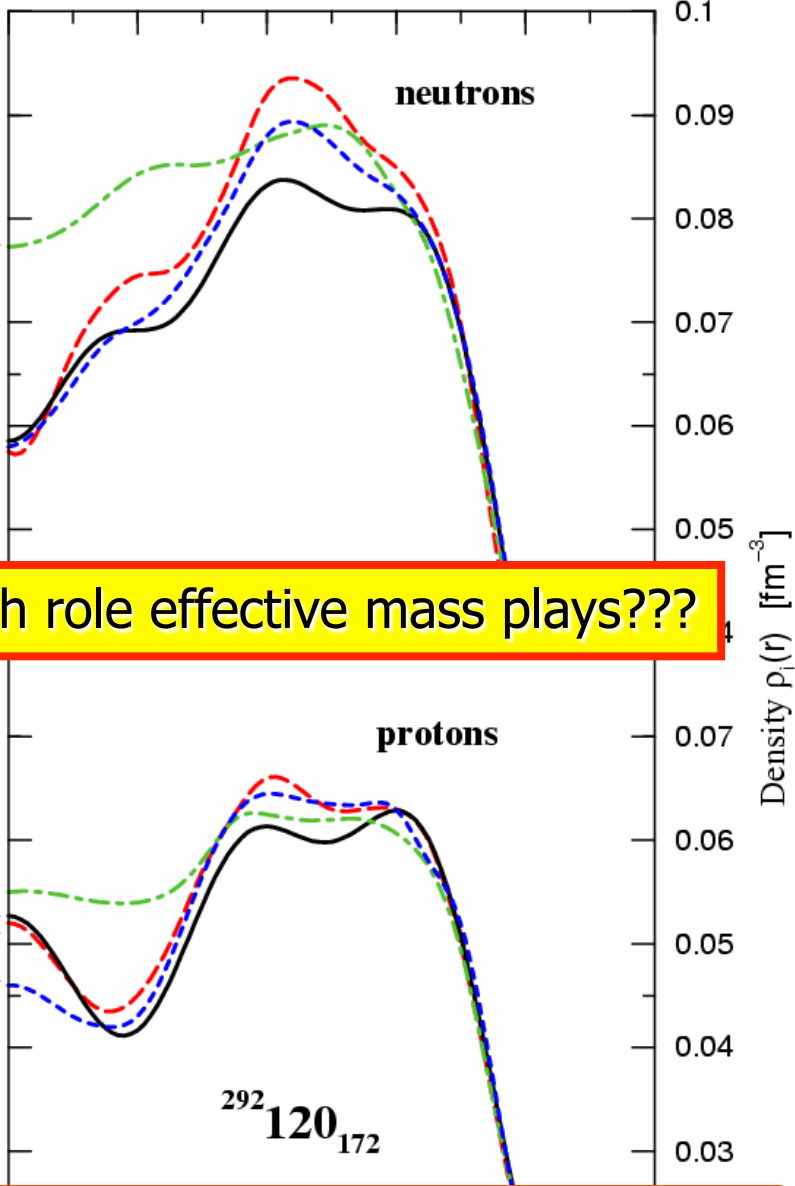
Skyrme SkI3 [$m^*/m=0.57$]
gaps at $Z=120, N=184$
 no double shell closure,
 SLy6

Gogny D1S
 $Z=120, N=172(?)$
 $Z=126, N=184$

CDFT
**double shell closure
 at $Z=120, N=172$**

Large effective
 mass $m^*/m \sim 0.8-1.0$

Low effective mass
 $m^*/m \sim 0.65$



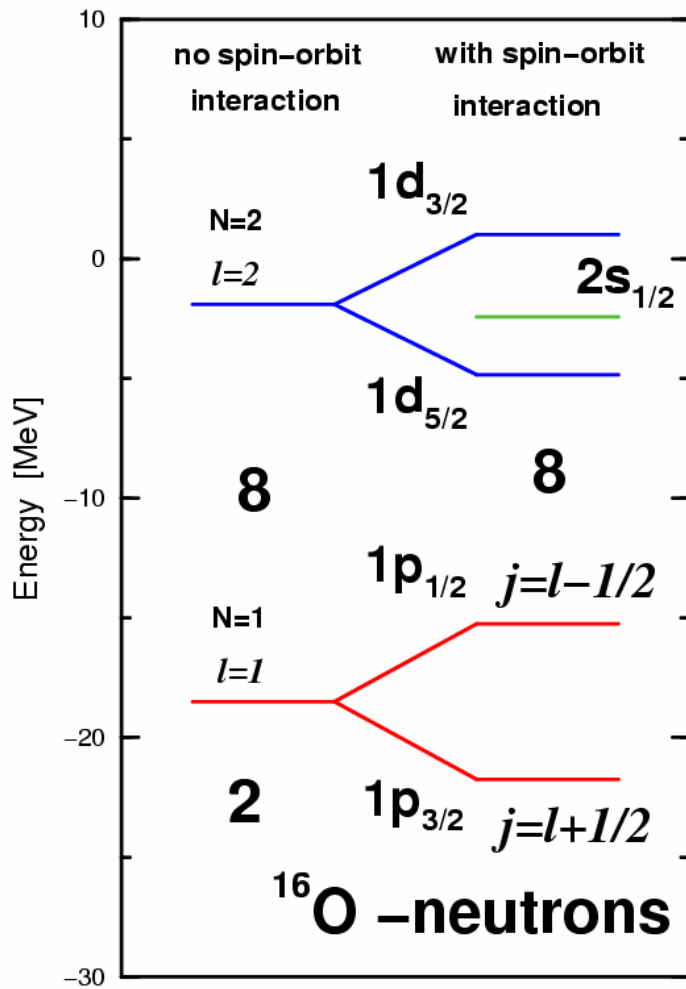
Which role effective mass plays???

RHB: Densities in paired and unpaired calculations are almost the same

Spin – orbit interaction – fully relativistic phenomenon

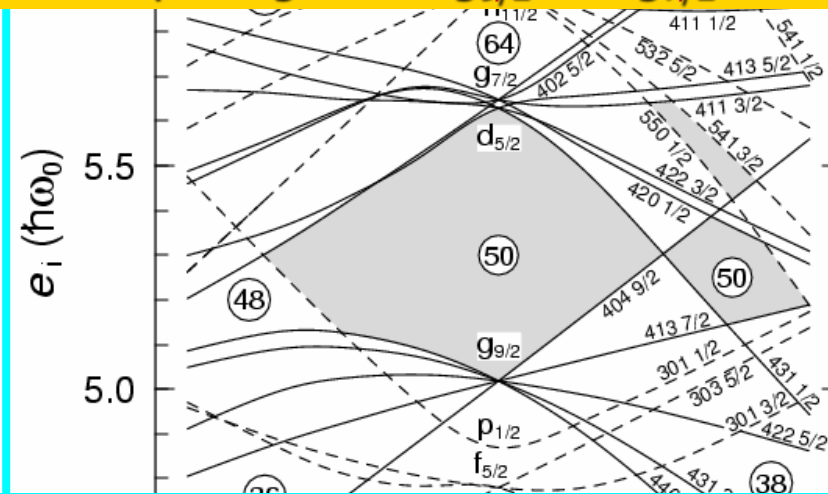
$$j = l \pm 1/2$$

$$V_{LS} = W(r)\vec{l}\vec{s}$$



Extremely important in medium and heavy mass nuclei

The Z=N=50 spherical shell gap is defined by the spin-orbit splitting of the g_{9/2} and g_{7/2} orbits



Without spin-orbit interaction:

1. Z=N=40 would be spherical shell gap
2. Sn (Z=50) nuclei will not be spherical in ground state

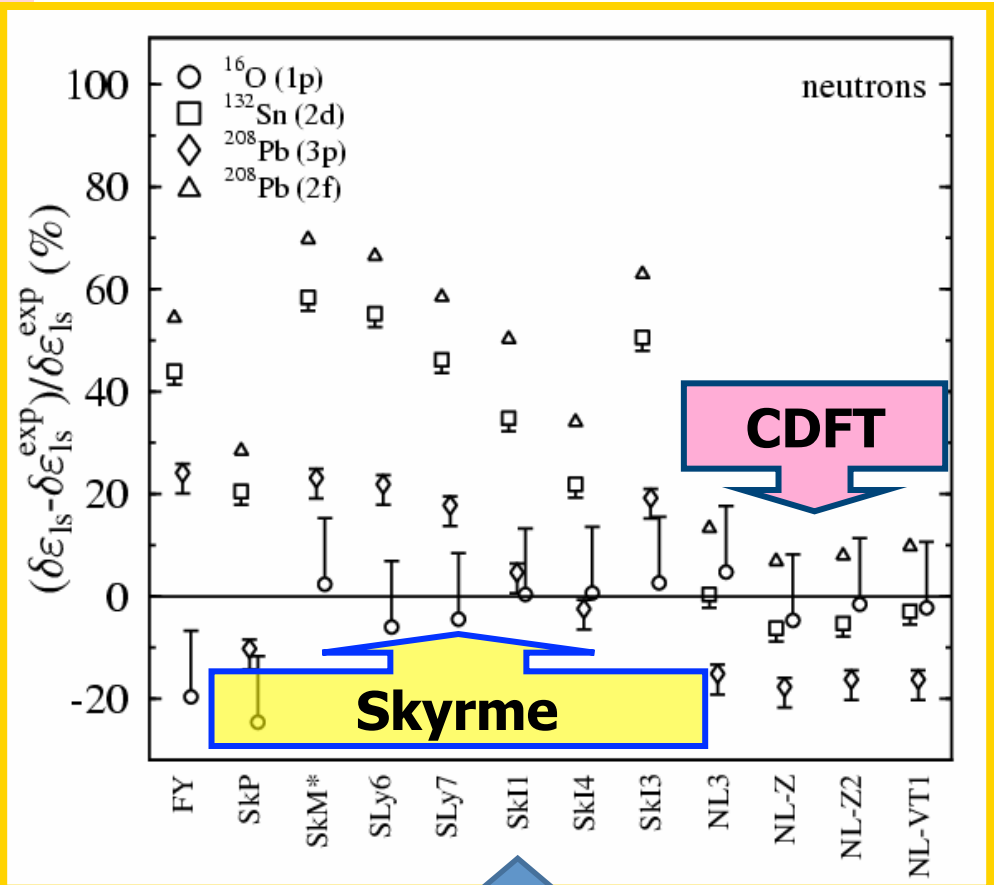
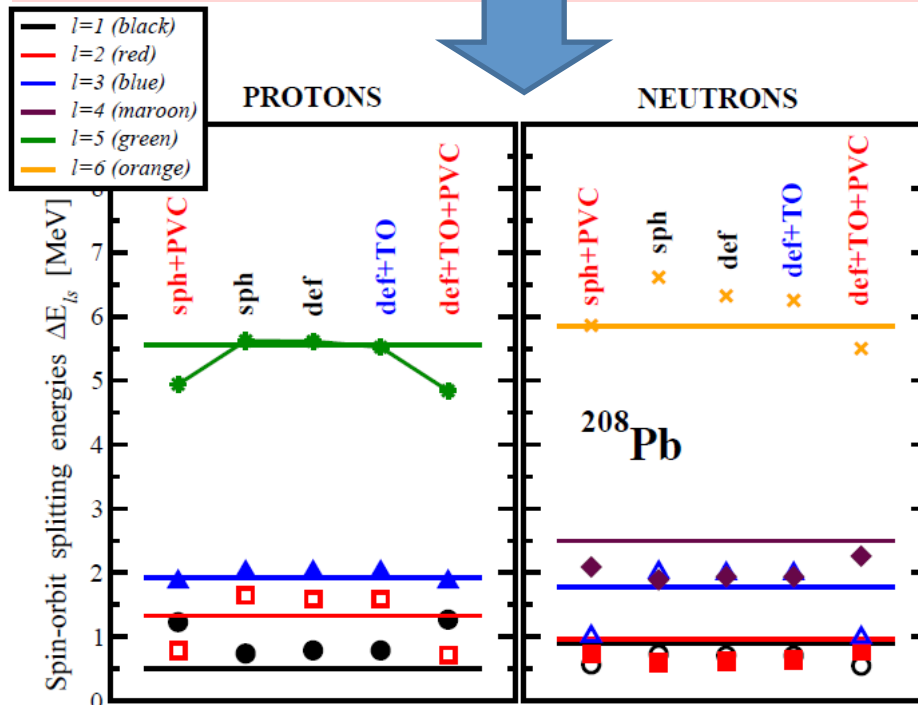
Spin-orbit splittings

Spin degrees of freedom as well as **spin-orbit interaction** are obtained in a natural way (no extra parameters) in the framework based on the Dirac equation (CDFT).

Spin-orbit splittings are properly described.

CDFT+PVC level

E.Litvinova, AA, PRC84, 014305(2011).



DFT - level

M.Bender et al, PRC60, 034304 (1999)

Need for accurate description of fission barriers since they strongly affect:

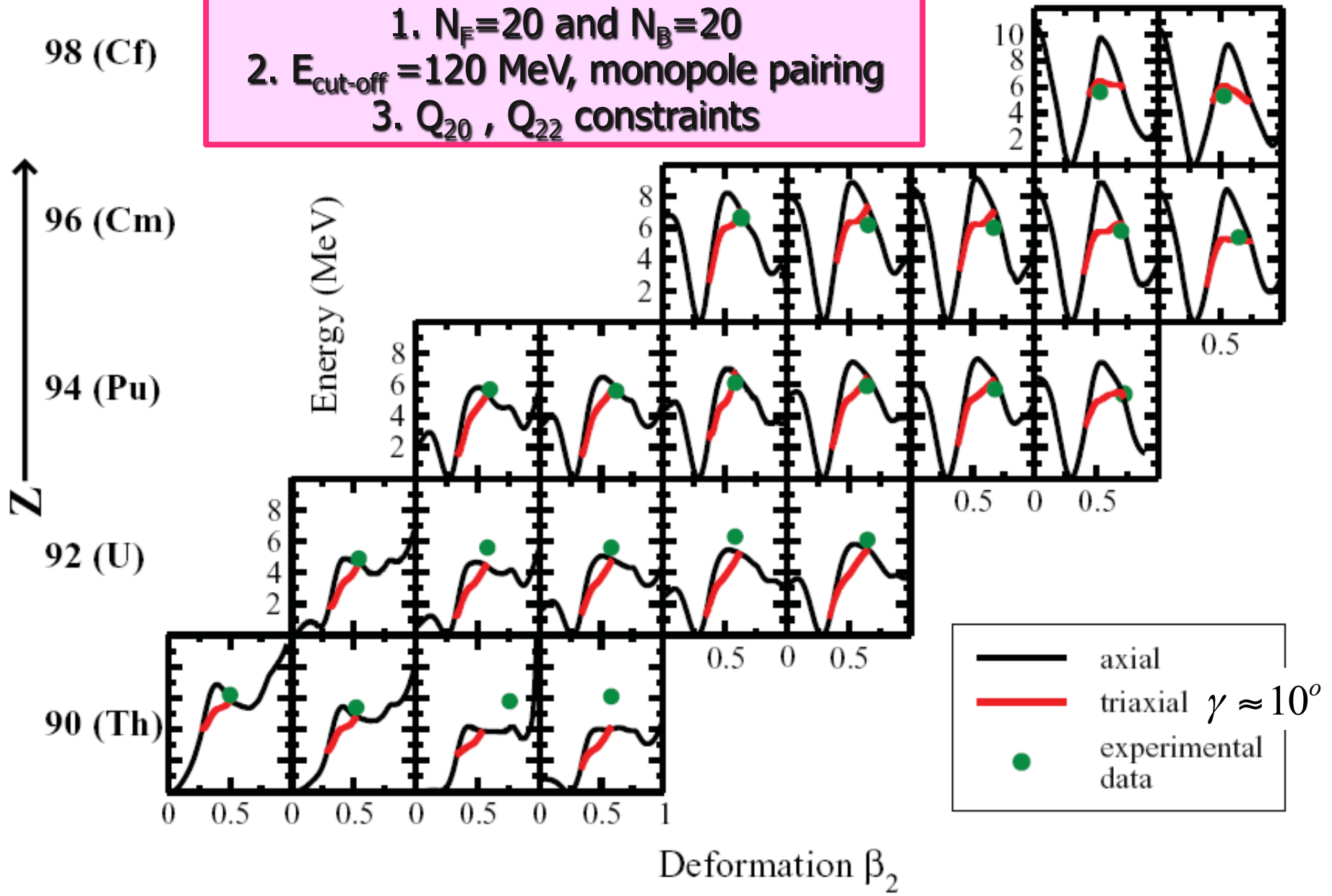
1. The probability for the **formation** of superheavy nuclei in heavy-ion-fusion reaction (the cross-section very sensitively depends on the fission barrier height).
- 2. survival probability** of an excited nucleus in its cooling by emitting neutrons and γ -rays in competition with fission (the changes in fission barrier height by 1 MeV changes the calculated survival probability by about one order of magnitude or more)
3. **spontaneous fission lifetimes**

RMF(NL3*)+BCS

$\xrightarrow{\quad N \quad}$

138 140 142 144 146 148 150 152 154

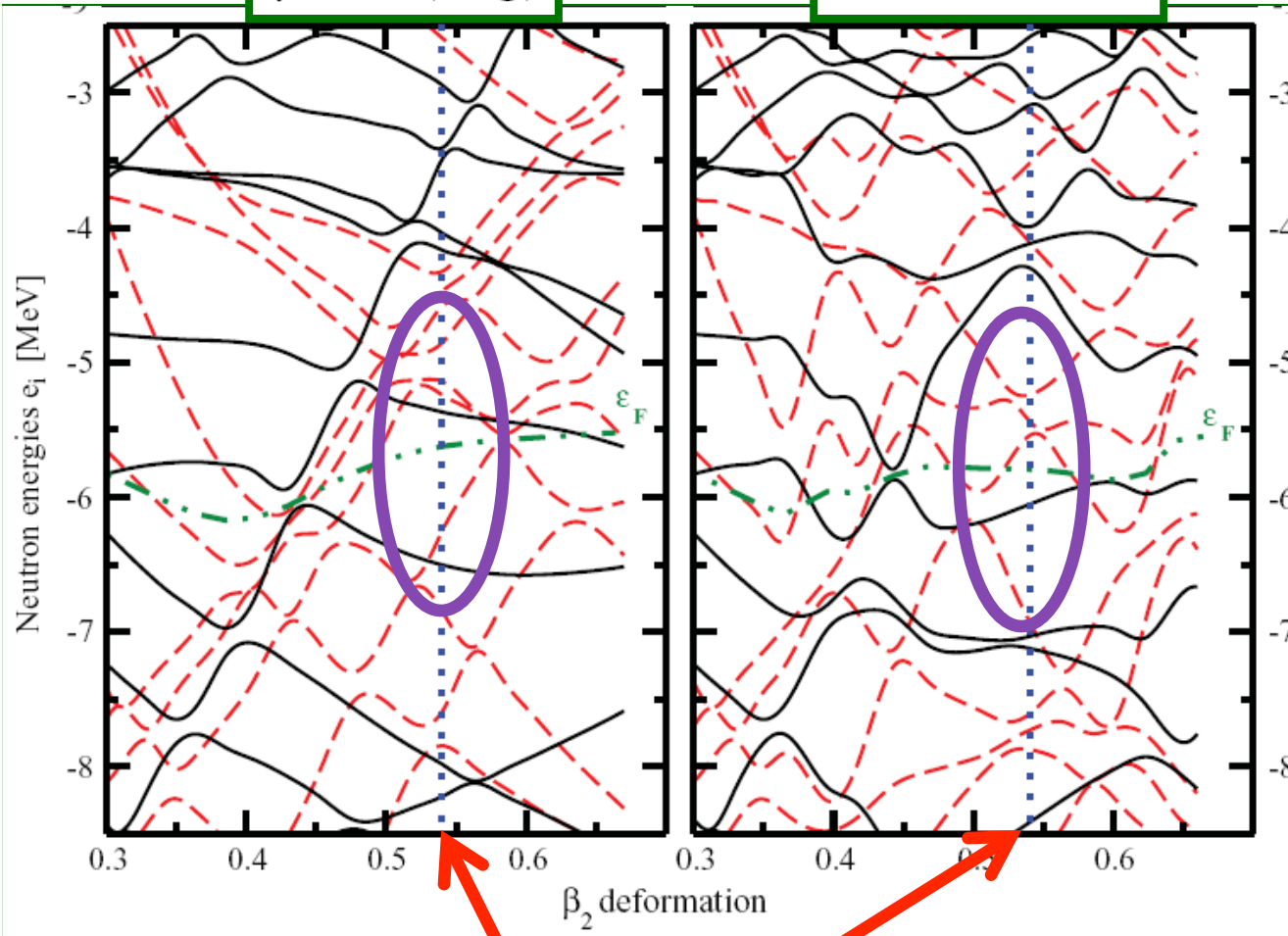
1. $N_F=20$ and $N_B=20$
2. $E_{\text{cut-off}}=120$ MeV, monopole pairing
3. Q_{20} , Q_{22} constraints



The microscopic origin of the lowering of the barrier due to triaxiality

$\gamma = 0$ (deg)

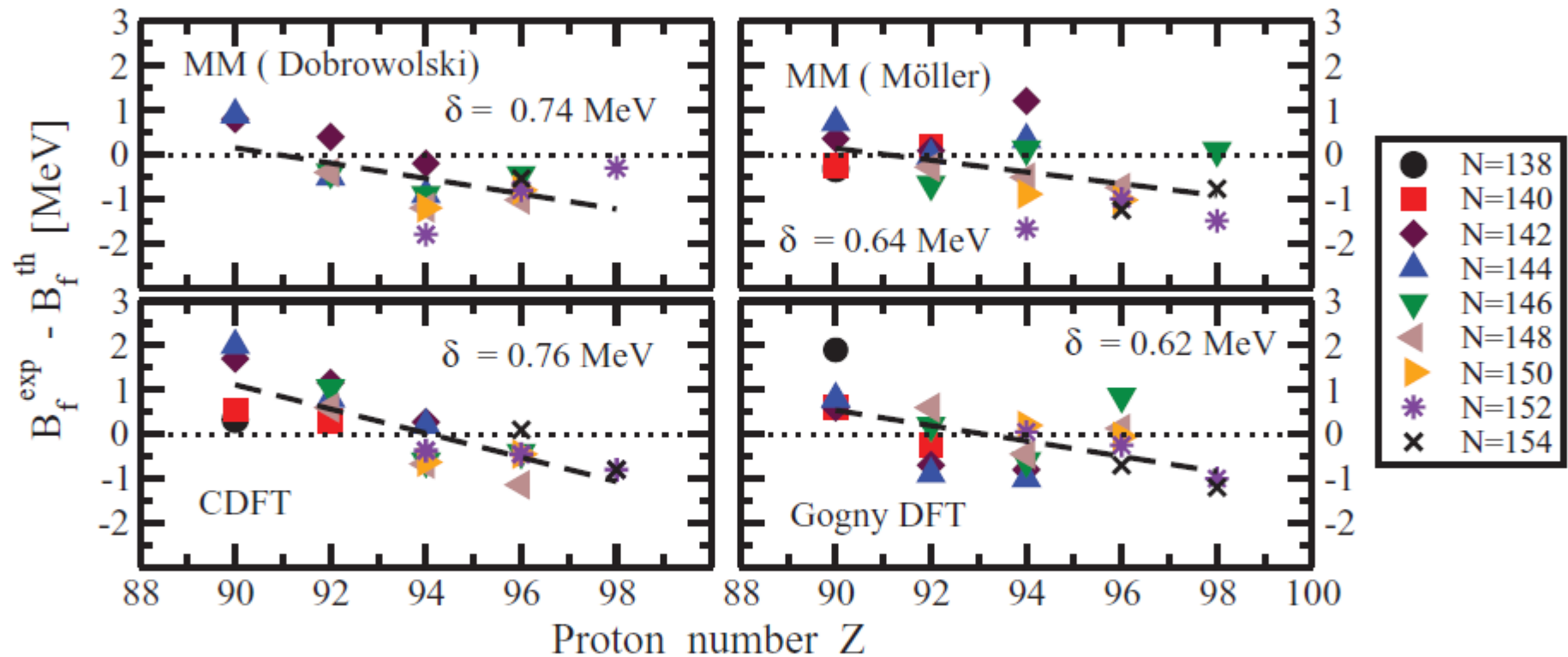
$\gamma \sim 10$ (deg)



The lowering of the level density at the Fermi surface induced by triaxiality leads to a more negative shell correction energy (as compared with axially symmetric solution), and, as a consequence, to a lower fission barrier.

the deformation of the saddle point

Fission barriers: theory versus experiment [state-of-the-art]

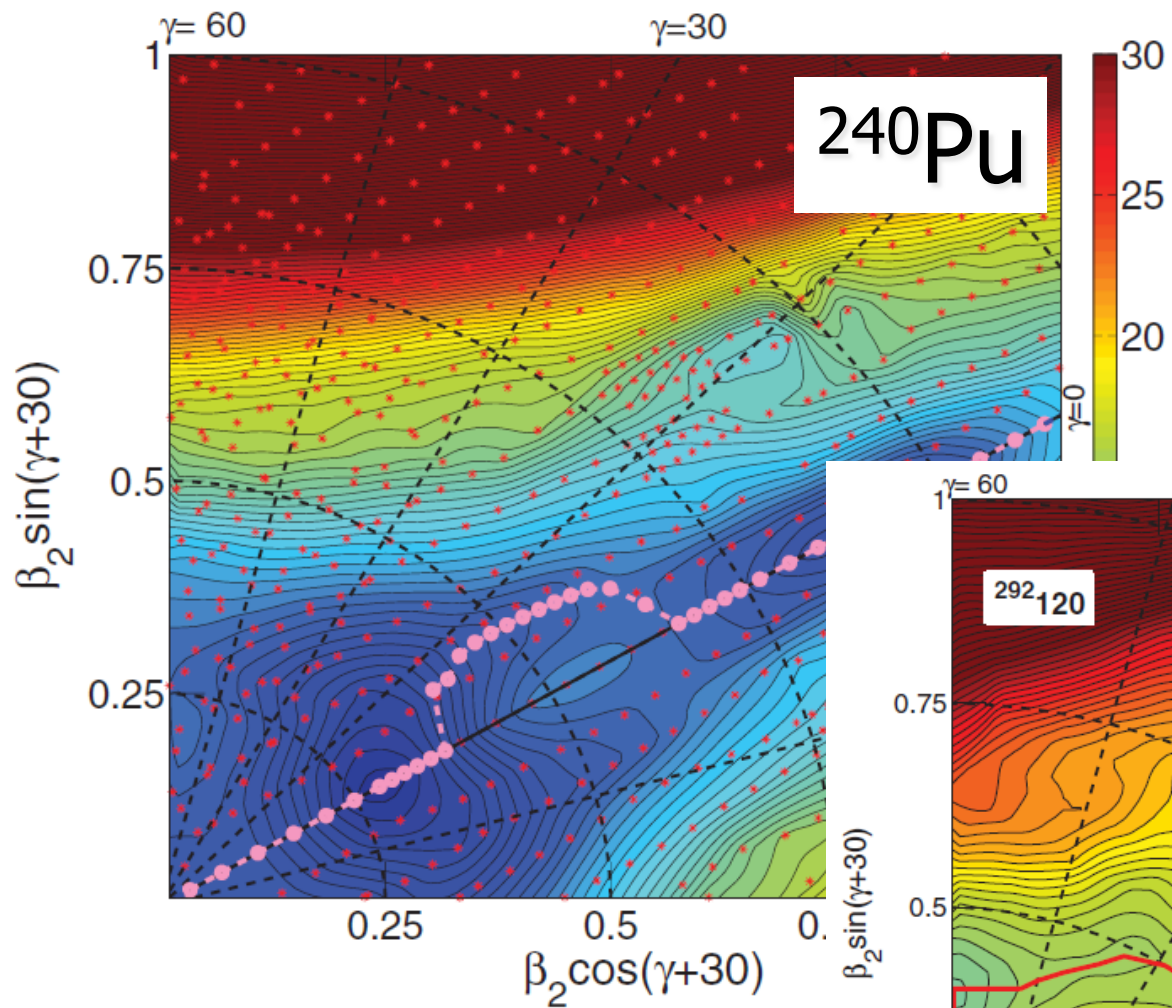


Mac+mic, LSD model
A. Dobrowolski et al,
PRC 75, 024613 (2007)

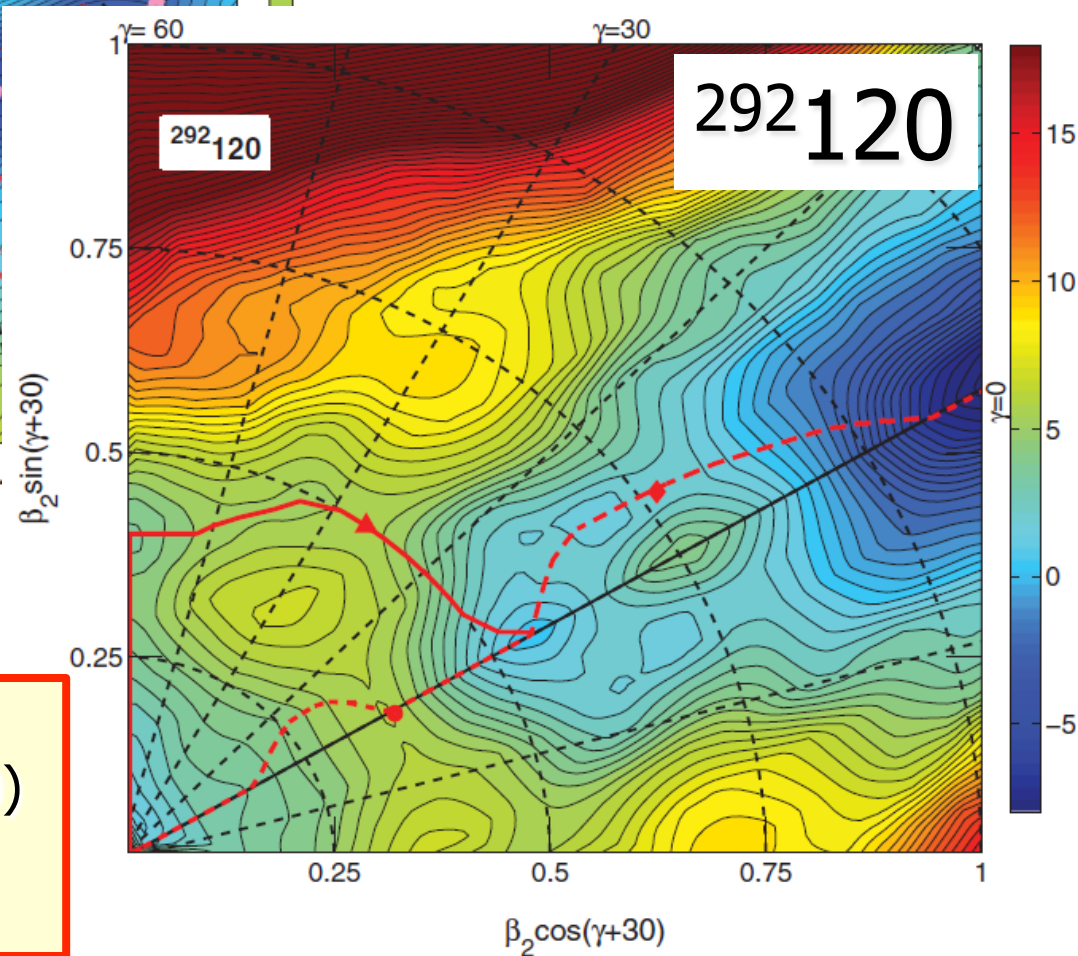
Mac+mic, FRDM model
P. Moller et al,
PRC 79, 064304 (2009)

Gogny DFT,
J.-P. Delaroche et al,
NPA 771, 103 (2006).

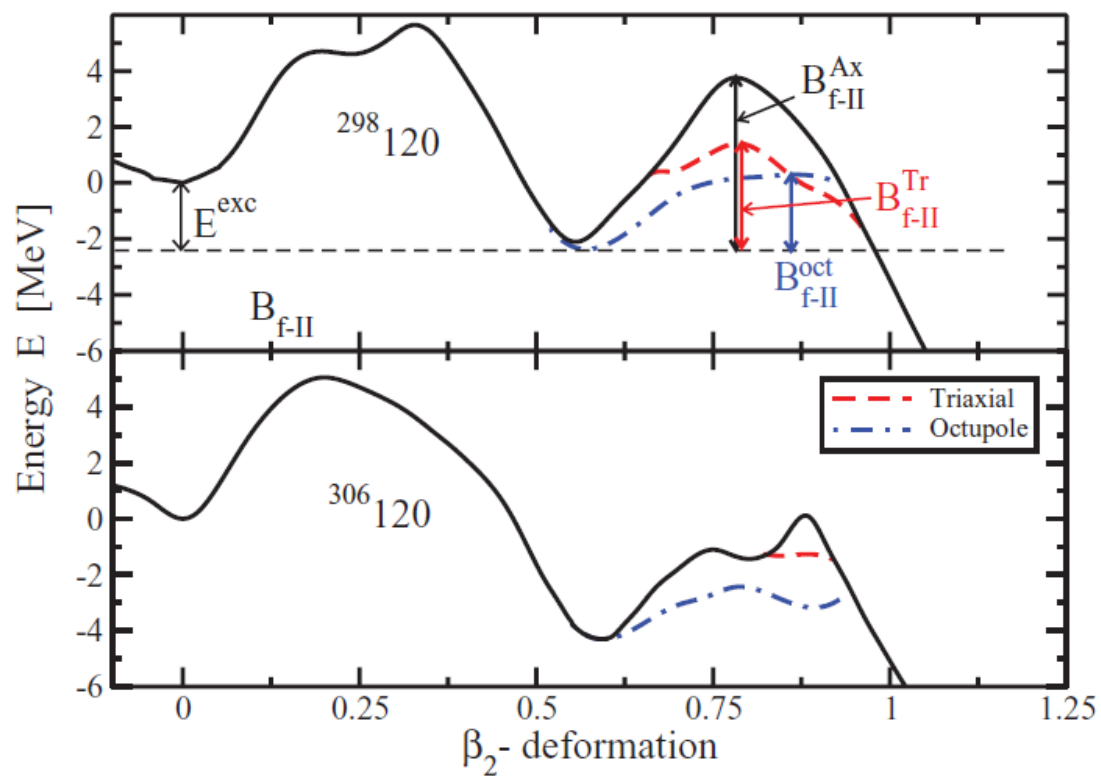
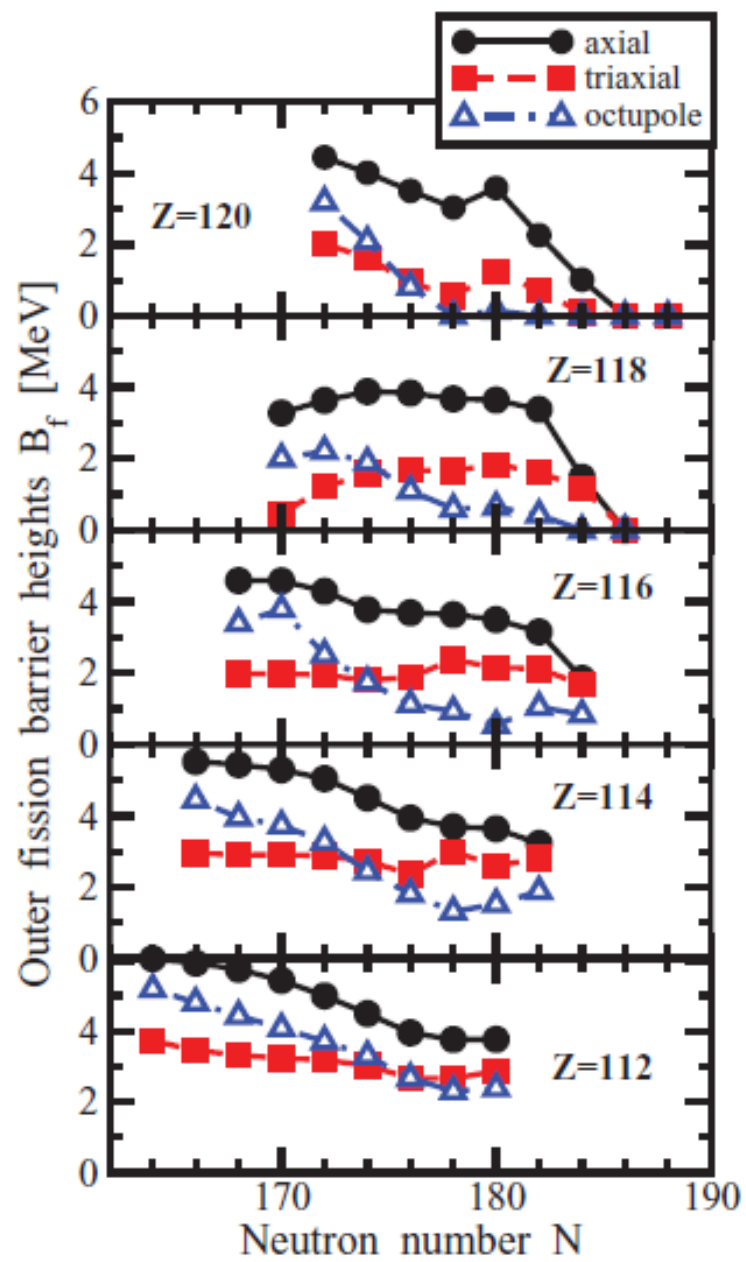
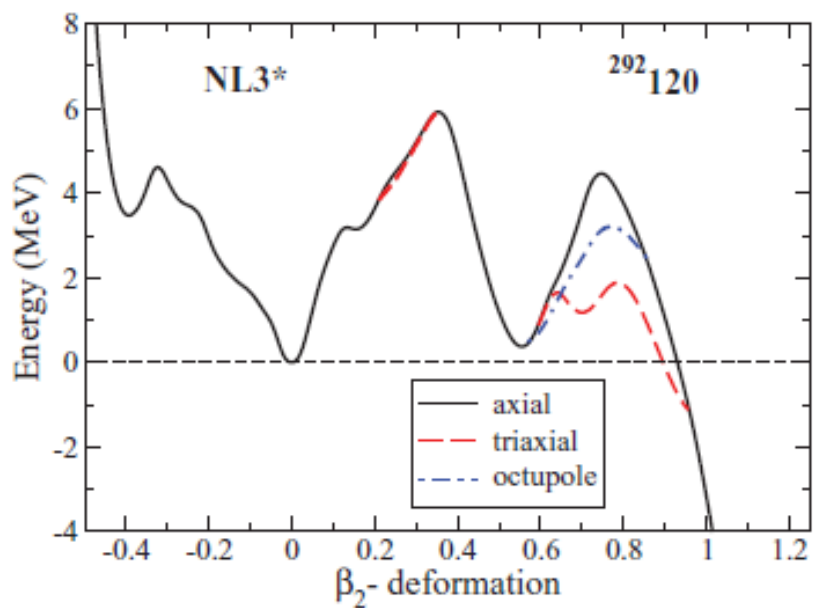
CDFT : actinides H. Abusara, AA and P. Ring, PRC 82, 044303 (2010)
superheavies: H. Abusara, AA and P. Ring, PRC 85, 024314 (2012)



**Triaxiality of fission barriers:
the origin**



H. Abusara, AA and P. Ring
actinides: PRC 82, 044303 (2010)
superheavies: PRC 85, 024314
(2012)

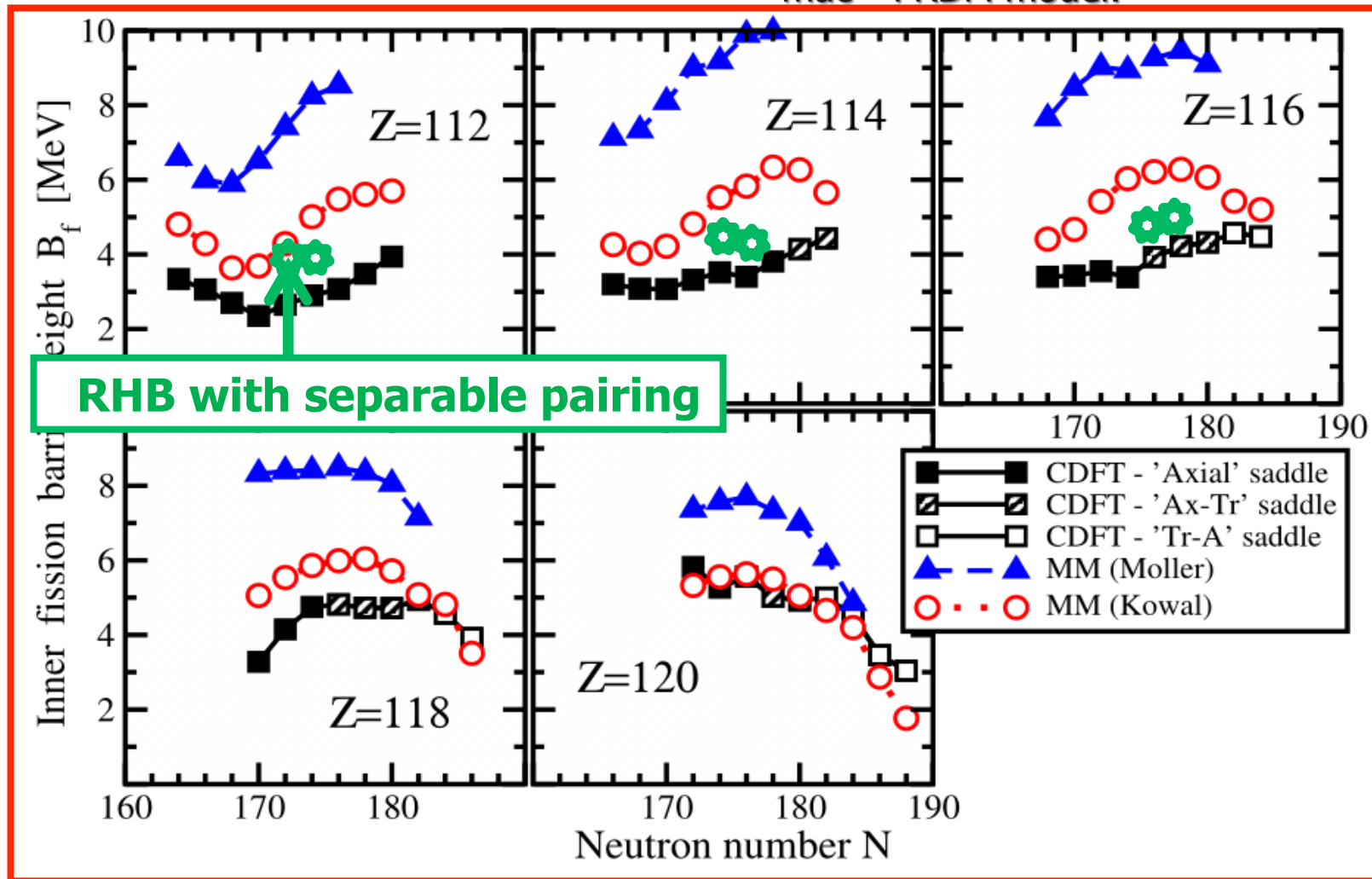


M. Kowal et al, PRC 82, 014303 (2010) - mic=WS potential,

mac=Yukawa+exponential model

P. Moller et al, PRC 79, 064304 (2009) – mic=Folded Yukawa potential

mac =FRDM model.



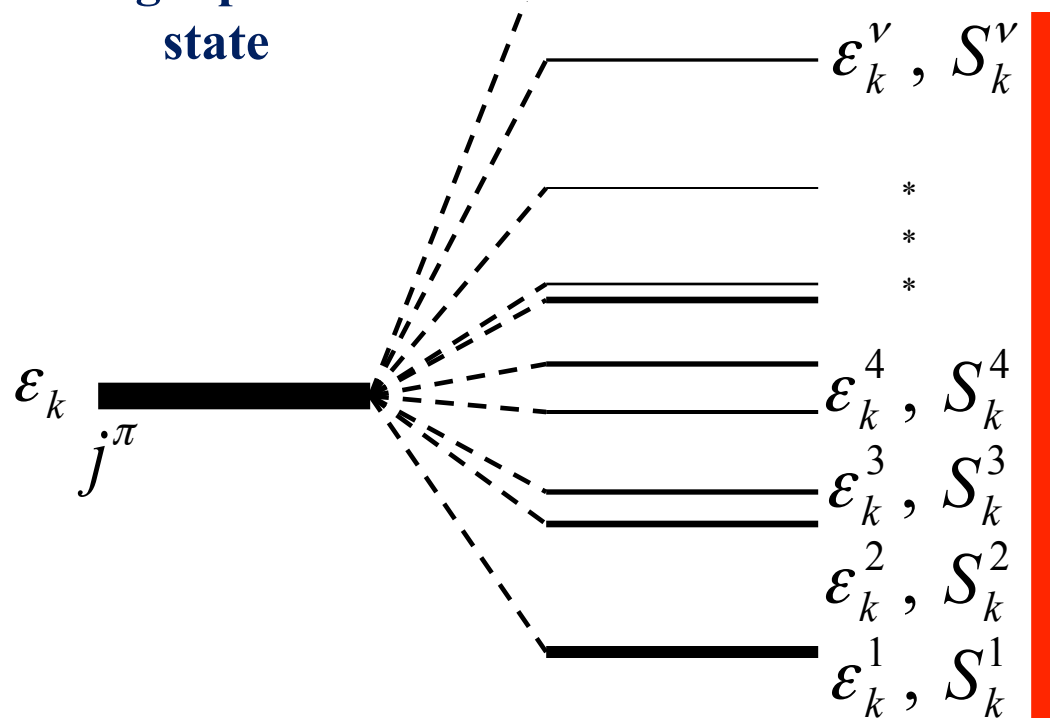
Inner fission barrier heights according to different models

Going beyond mean field approximation:
particle-vibration coupling in spherical
nuclei

The single particle states are fragmented

Mean-field
single-particle
state

Fragmented levels
(due to coupling to phonons)



METHOD 1.

$$\epsilon_k^{grav} = \left[\sum_{\nu} S_k^{\nu} \cdot \epsilon_k^{\nu} \right] / \left[\sum_{\nu} S_k^{\nu} \right]$$

This energy is associated with a “bare” single-particle energy.

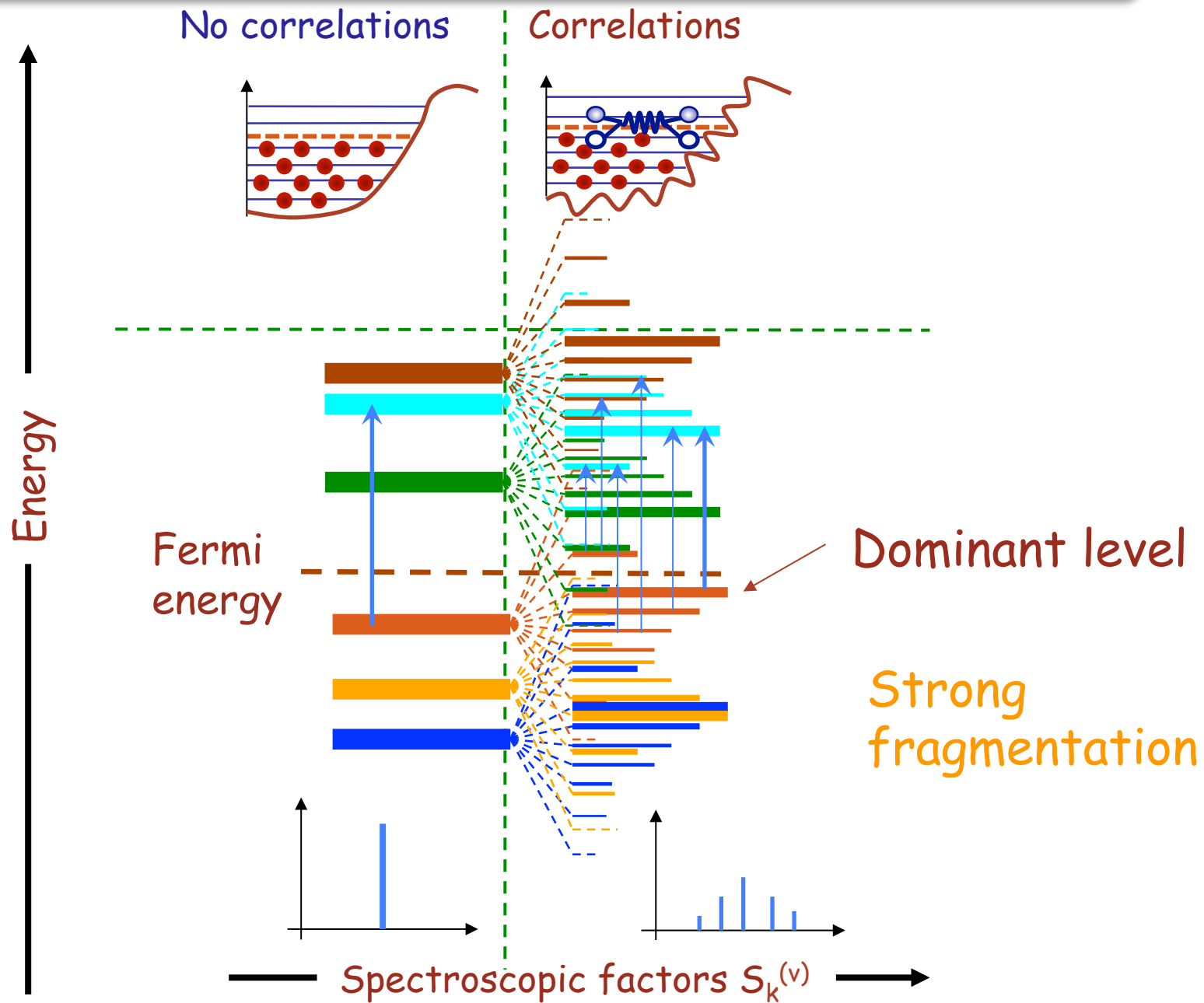
Spectroscopic factors depend on reaction and method of extraction:
example of spectroscopic factors
in ^{209}Bi

1. Spins and parities of fragments are frequently not measured.
2. Some fragments are not observed.
3. Sum rule $\sum_{\nu} S_k^{\nu} = 1$ is frequently violated.

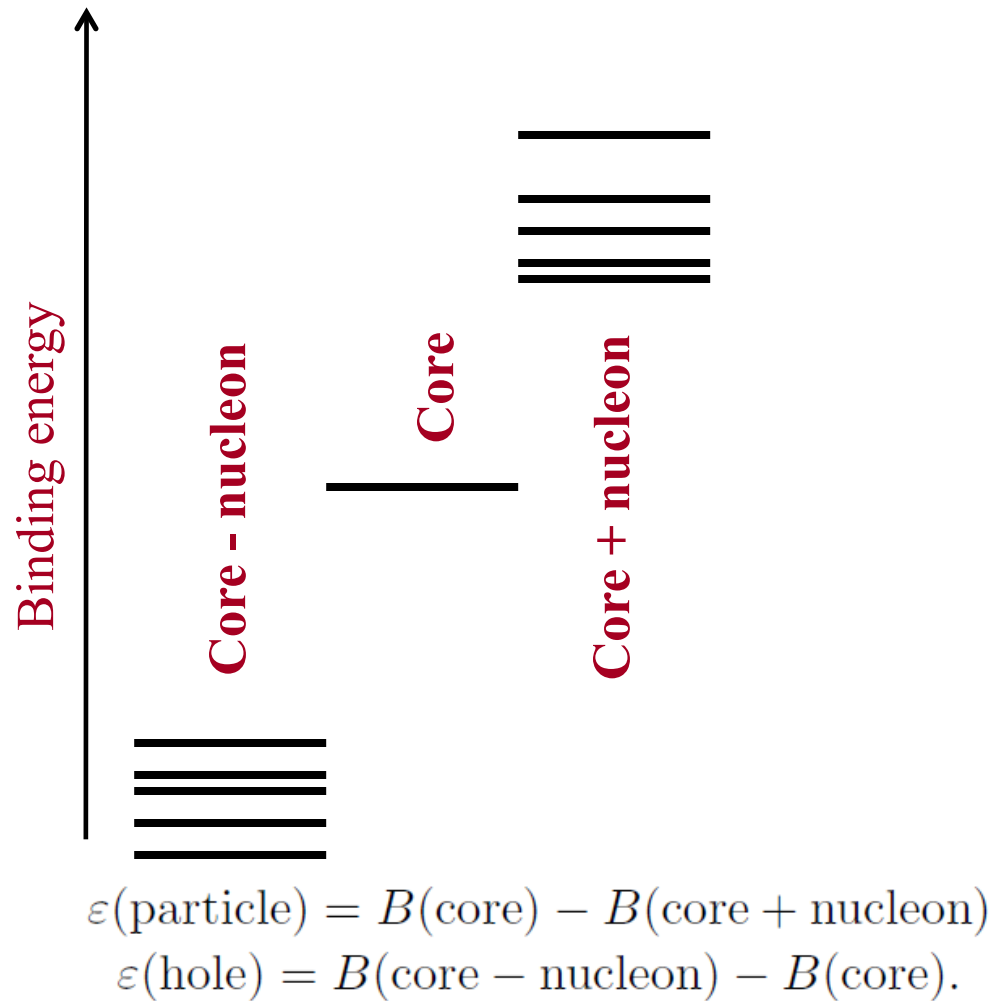
| | | |
|--------------------|------|------|
| 1h _{9/2} | 1.17 | 0.80 |
| 2f _{7/2} | 0.78 | 0.76 |
| 1i _{13/2} | 0.56 | 0.74 |
| 2f _{5/2} | 0.88 | 0.57 |
| 3p _{3/2} | 0.67 | 0.44 |
| 3p _{1/2} | 0.49 | 0.20 |

($^3\text{He},d$) (α,t) reactions

The single particle states are fragmented

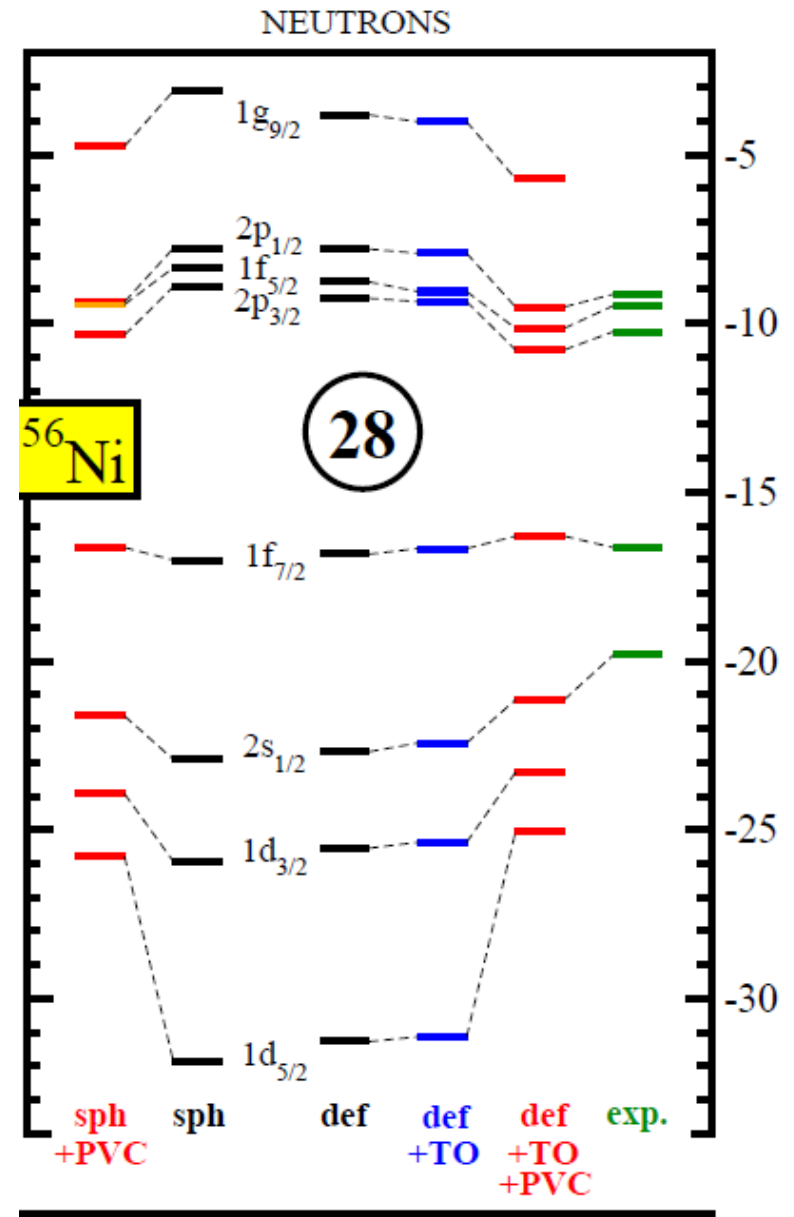


How single-particle spectra are obtained in experiment



Include **polarization effects due to**

1. **deformation (def) and**
2. **time-odd (TO) mean fields as well as**
3. **energy corrections due to particle-vibration coupling (PVC)**



Relativistic particle-vibration coupling (PVC) model

The equation of the one-nucleon motion has the form (in single-particle Green functions)

$$(\varepsilon - h^D - \beta \Sigma_s^e(\varepsilon) - \Sigma_0^e(\varepsilon)) G(\varepsilon) = 1.$$



$$\sum_l \{(\varepsilon - \varepsilon_k) \delta_{kl} - \Sigma_{kl}^e(\varepsilon)\} G_{lk'}(\varepsilon) = \delta_{kk'}$$

particle-phonon coupling model:

energy-dependent part of the mass operator is a convolution of the particle-phonon coupling amplitude Γ and the exact single-particle Green's function

$$\Sigma_{kl}^e(\varepsilon) = \sum_{k'l'} \int_{-\infty}^{+\infty} \frac{d\omega}{2\pi i} \Gamma_{kl'lk'}(\omega) G_{k'l'}(\varepsilon + \omega).$$

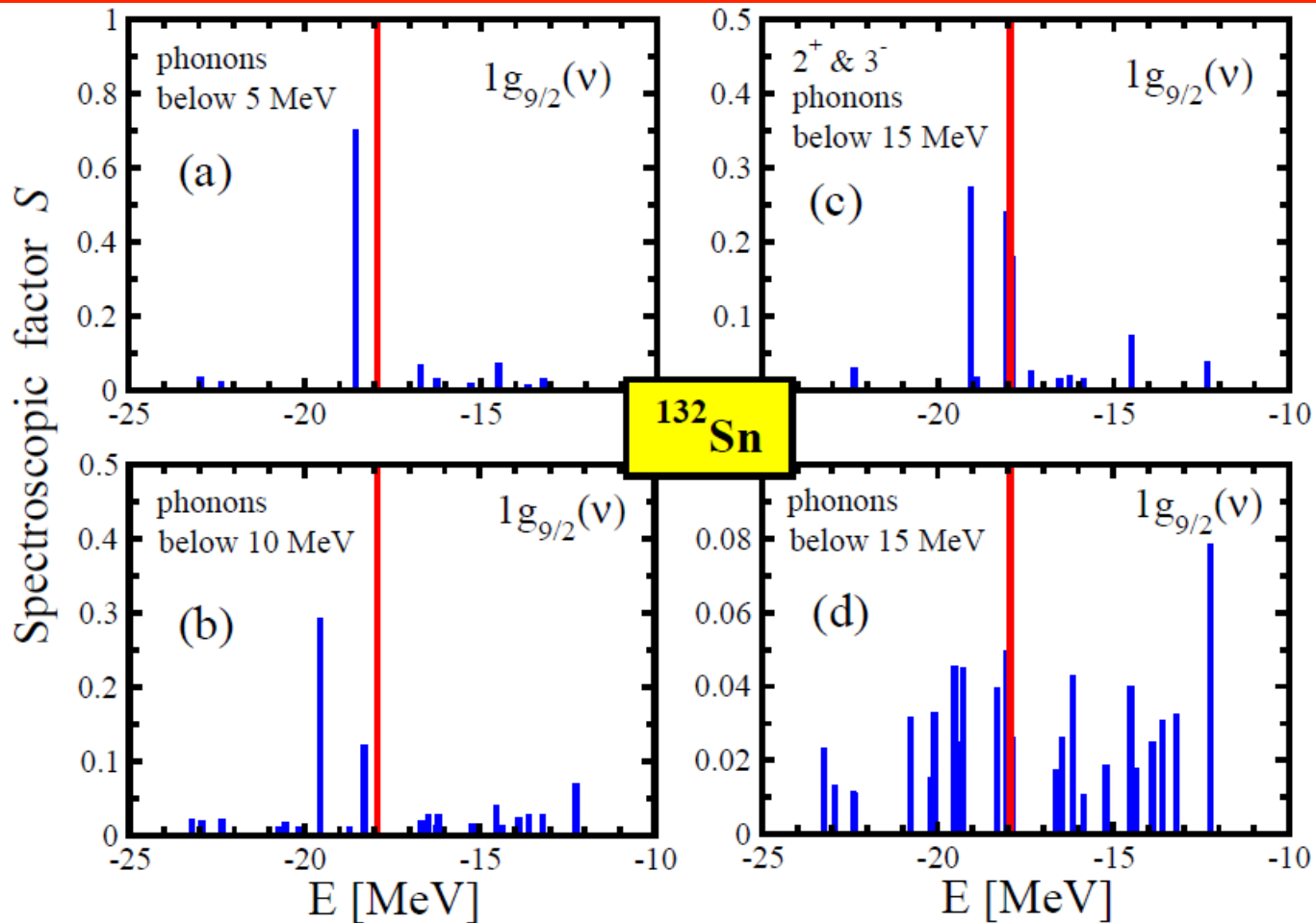


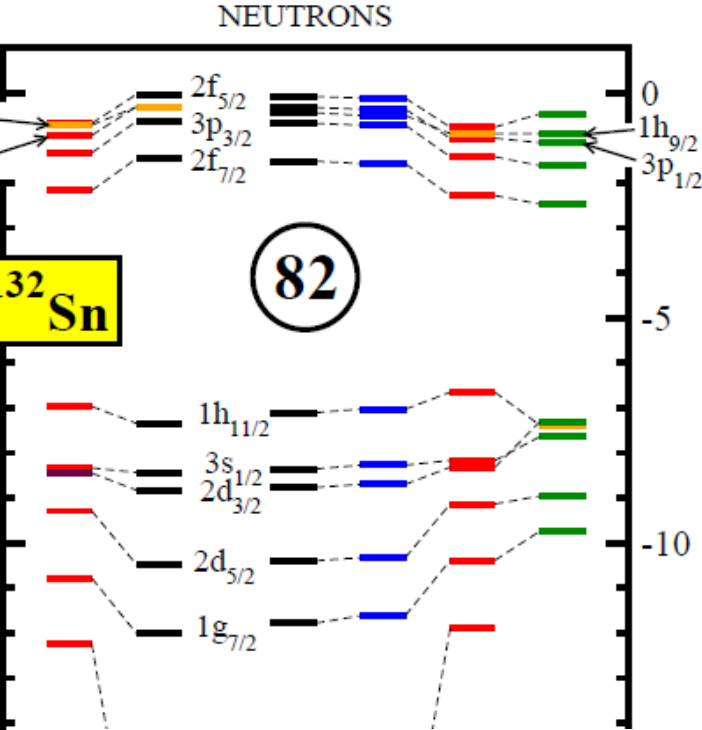
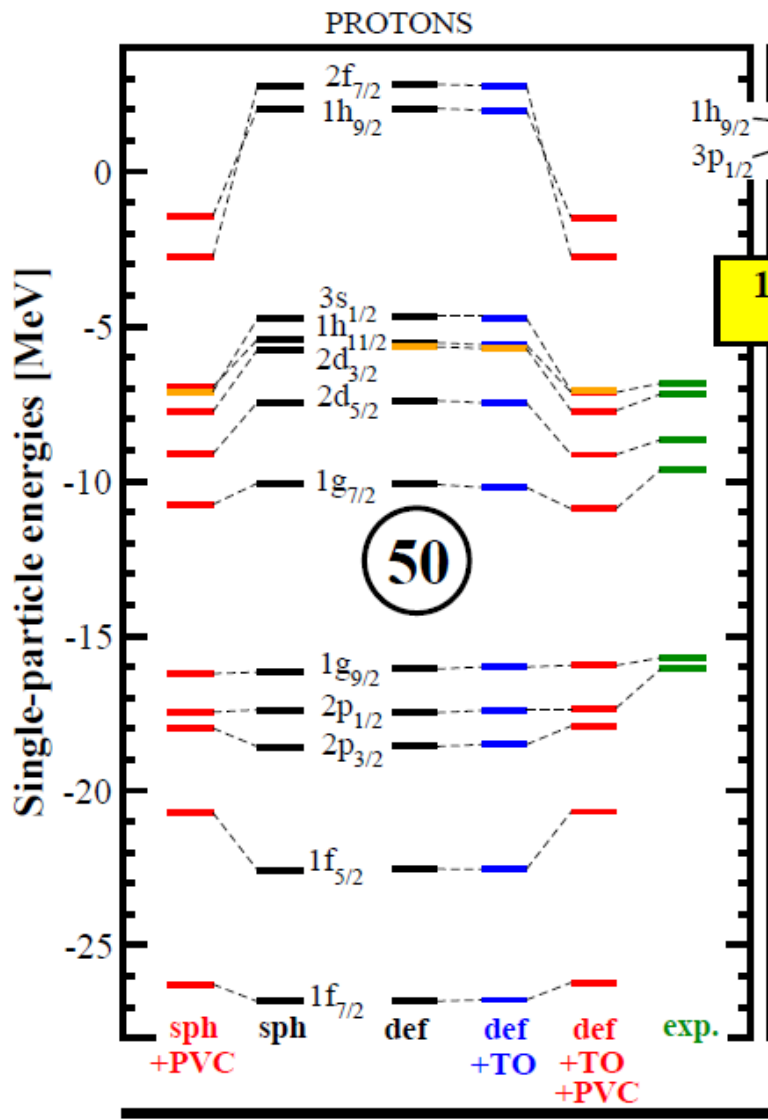
depends on phonon vertexes $\gamma_{kl}^\mu = \sum_{k'l'} V_{kl'lk'} \delta\rho_{k'l'}^\mu$

$V_{kl'lk'}$ - the relativistic matrix element of the residual interaction and $\delta\rho$ is the transition density. We use the linearized version of the model which assumes that $\delta\rho$ is not influenced by the particle-phonon coupling and can be computed within relativistic RPA.

Cut-off of phonon basis in the RRPA calculations

Phonons of the multiplicities 2^+ , 3^- , 4^+ , 5^- , 6^+ with energies below 15 MeV are included in the model space of the PVC calculations. The addition of phonon modes with energies above 15 MeV does not affect the results. The phonon energies and their coupling vertices have been computed within the self-consistent RRPA.





NL3*
functional

TABLE I: Average deviations per state $\Delta\epsilon$ between calculated and experimental energies of the single-particle states for a proton (neutron) subsystem of a given nucleus. The results

| Nucleus/subsystem | $\Delta\epsilon_{def+TO}$ [MeV] | $\Delta\epsilon_{def+TO+PVC}$ [MeV] |
|---------------------------|---------------------------------|-------------------------------------|
| ⁵⁶ Ni/proton | 0.76 | 0.77 |
| ⁵⁶ Ni/neutron | 0.89 | 0.71 |
| ¹³² Sn/proton | 1.02 | 0.68 |
| ¹³² Sn/neutron | 0.89 | 0.39 |
| ²⁰⁸ Pb/proton | 1.53 | 0.84 |
| ²⁰⁸ Pb/neutron | 1.00 | 0.47 |

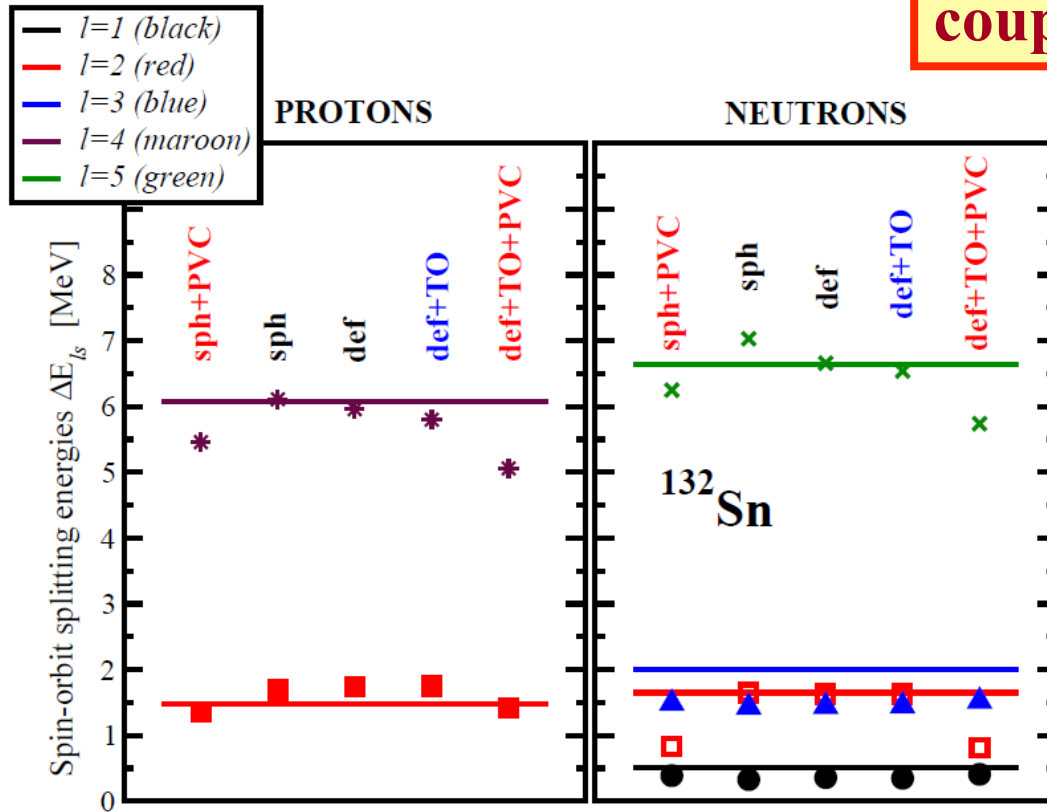
particle-vibration coupling
+ TO, TE polarization effects

Spectroscopic factors

| Nucleus | State | S_{th} | S_{exp} | S_{exp} |
|-------------------|-------------|----------|-----------------|-----------|
| ^{209}Bi | $1h_{9/2}$ | 0.88 | 1.17 [75] | 0.80 [69] |
| | $2f_{7/2}$ | 0.78 | 0.78 [75] | 0.76 [69] |
| | $1i_{13/2}$ | 0.63 | 0.56 [75] | 0.74 [69] |
| | $2f_{5/2}$ | 0.61 | 0.88 [75] | 0.57 [69] |
| | $3p_{3/2}$ | 0.62 | 0.67 [75] | 0.44 [69] |
| | $3p_{1/2}$ | 0.37 | 0.49 [75] | 0.20 [69] |
| | | | | |
| Nucleus | State | S_{th} | S_{exp} | |
| ^{133}Sn | $2f_{7/2}$ | 0.89 | 0.86 ± 0.16 | |
| | $3p_{3/2}$ | 0.91 | 0.92 ± 0.18 | |
| | $1h_{9/2}$ | 0.88 | | |
| | $3p_{1/2}$ | 0.91 | 1.1 ± 0.3 | |
| | $2f_{5/2}$ | 0.89 | 1.1 ± 0.2 | |

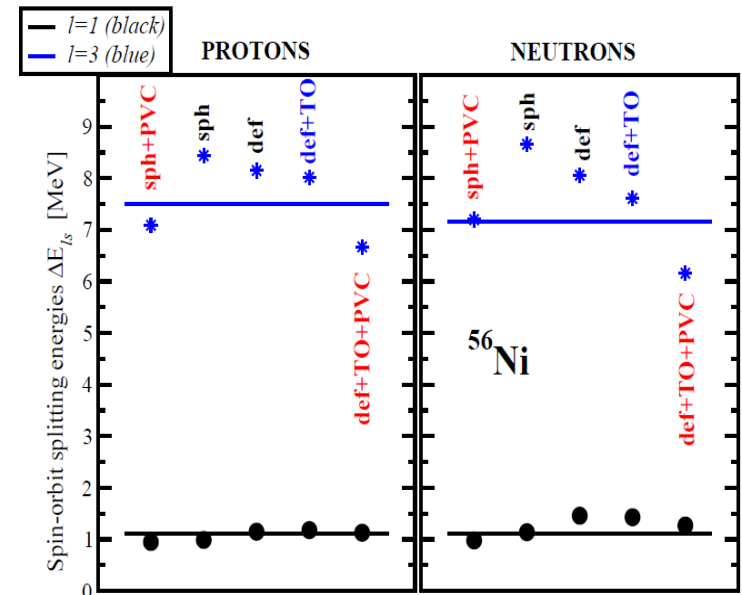
The absolute values of experimental spectroscopic factors are characterized by large ambiguities and depend strongly on the reaction employed in experiment and the reaction model used in the analysis

The impact of particle-vibration coupling on spin-orbit splittings.



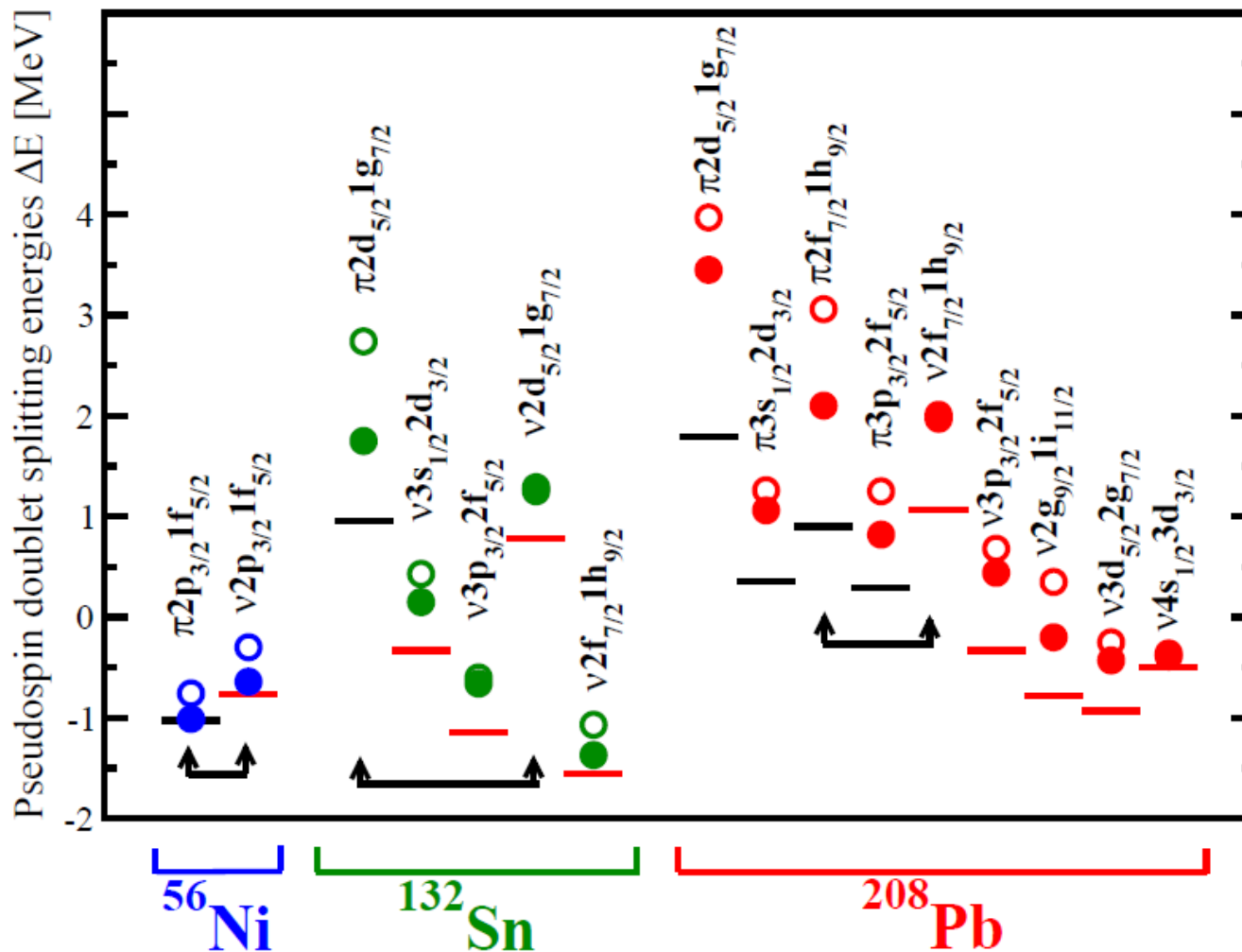
The absolute deviations per doublet are **0.34 MeV [0.50 MeV]**, **0.23 MeV [0.56 MeV]** and **0.26 MeV [0.45 MeV]** in the **mean field (“def+TO”)** [particle-vibration coupling (“def+TO+PVC”)] calculations in ^{56}Ni , ^{132}Sn and ^{208}Pb , respectively.

The inclusion of particle-vibration coupling **decreases** the accuracy of the description of spin-orbit splittings.



The impact of particle-vibration coupling on pseudospin doublets.

$$\Delta E = E_{n_r, l, j=l+1/2} - E_{(n_r-1), (l+2), j=l+3/2}.$$



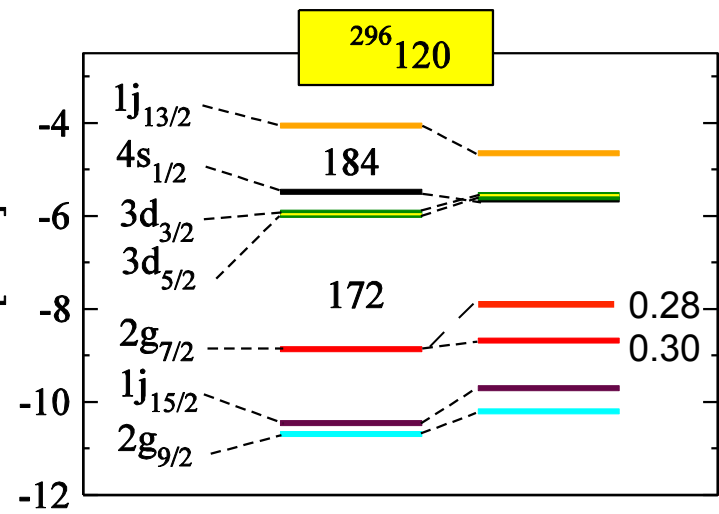
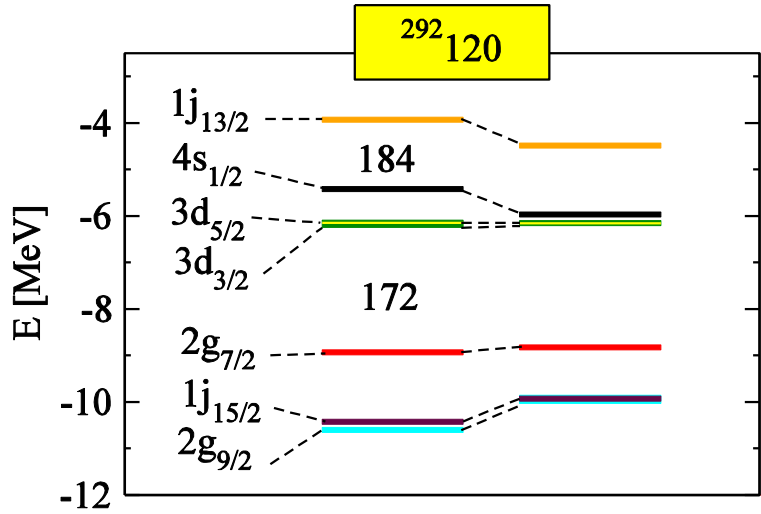
— Exp (protons)
 — Exp (neutrons)

○ def+TO
 ● def+TO+PVC

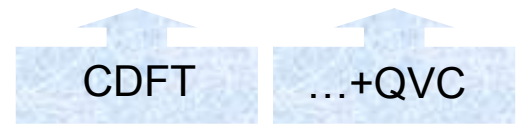
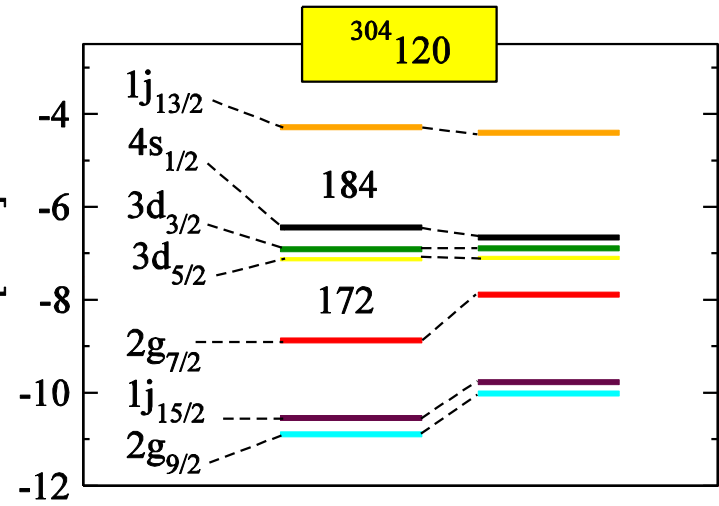
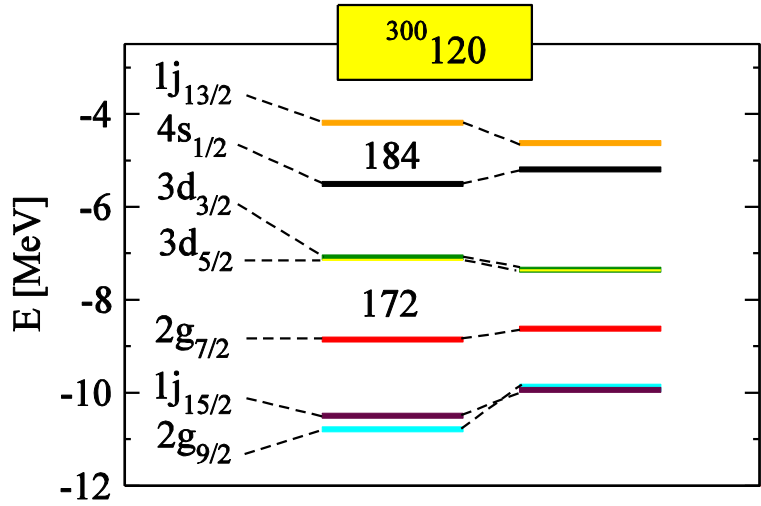
PVC substantially improves the description of splitting energies in pseudospin doublets as compared with mean field calculations.

Observed similarity of the splitting energies of proton and neutron pseudospin doublets with the same single-particle structure in medium and heavy mass nuclei can only be reproduced when the particle-vibration coupling is taken into account.

Dominant neutron states in $Z = 120$

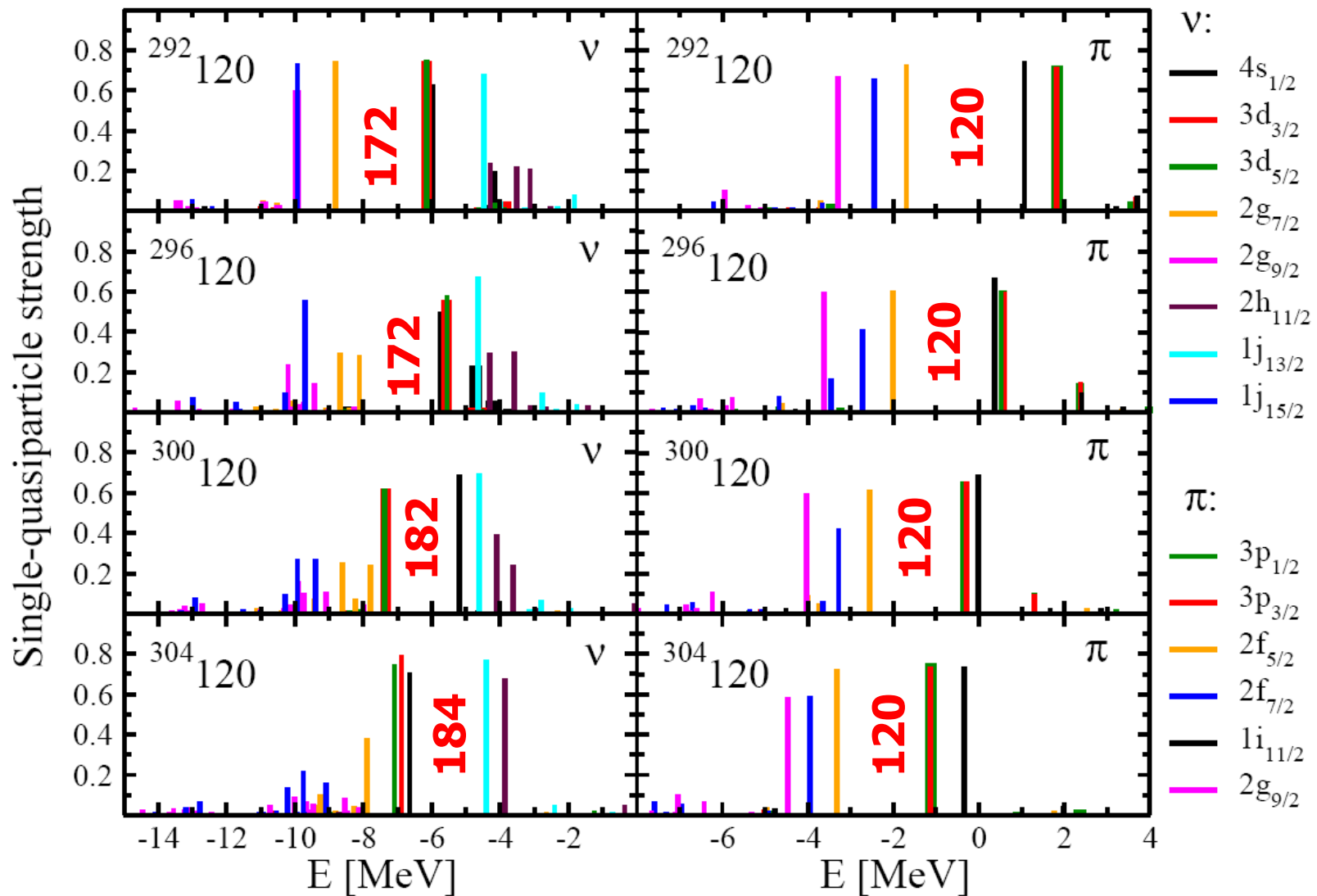


Comparable Spectroscopic strengths



Shell evolution in superheavy $Z = 120$ isotopes: Quasiparticle-vibration coupling (QVC) in a relativistic framework

E.Litvinova., PRC 85, 021303(R) (2012)

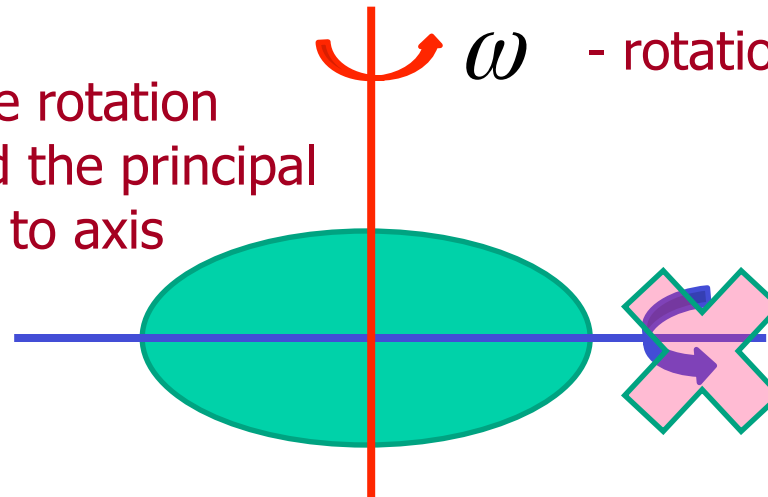


Rotating nuclei

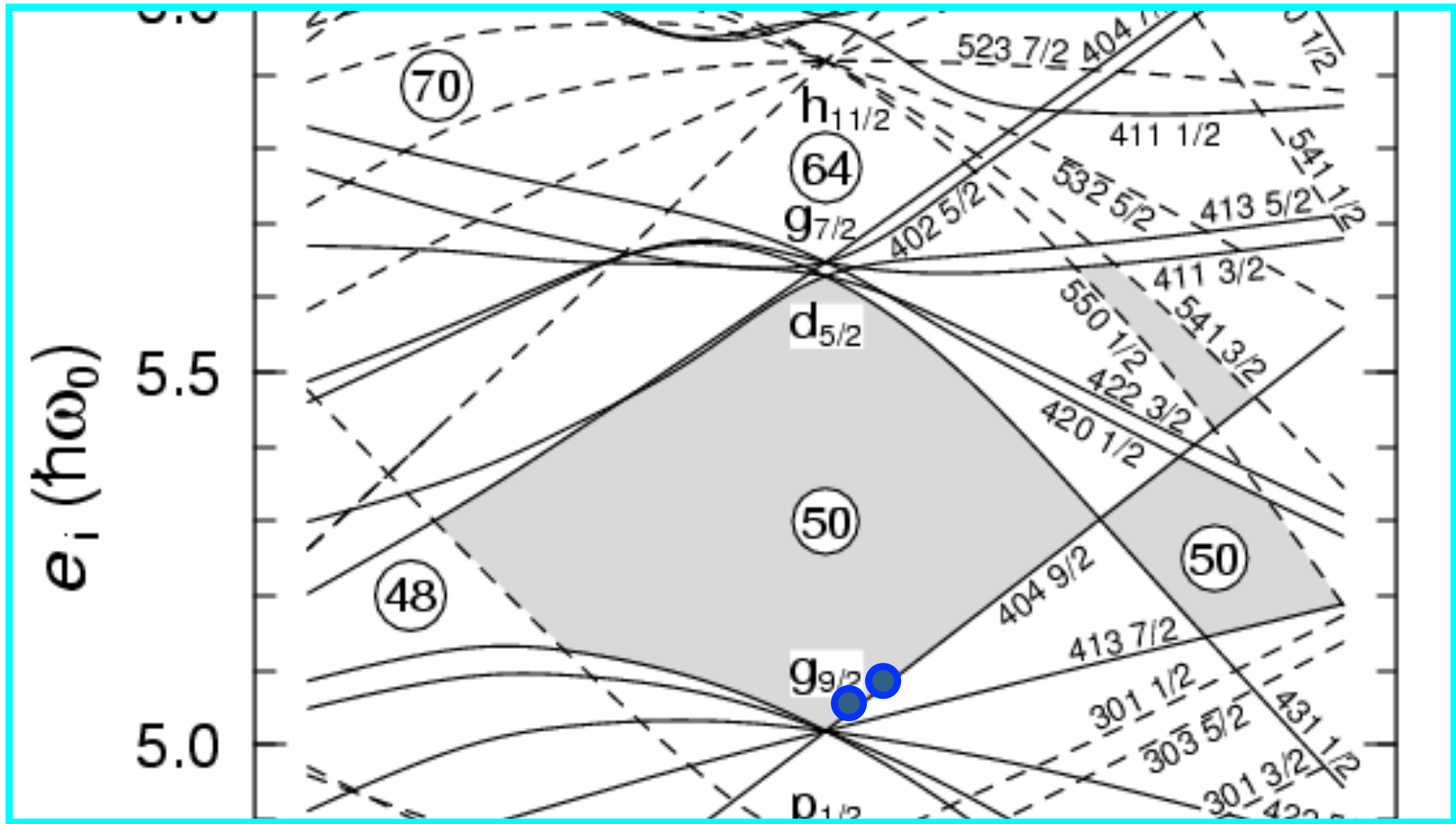
Major features of rotation

1. The nucleus has to be deformed to rotate (most nuclei have a deformed axial shape in the ground state)
2. The nucleus rotates as a whole → **collective** degrees of freedom
3. The nucleons move independently inside the deformed potential → **intrinsic (single-particle)** degrees of freedom
4. The nucleonic motion is much faster than the rotation → adiabatic approximation

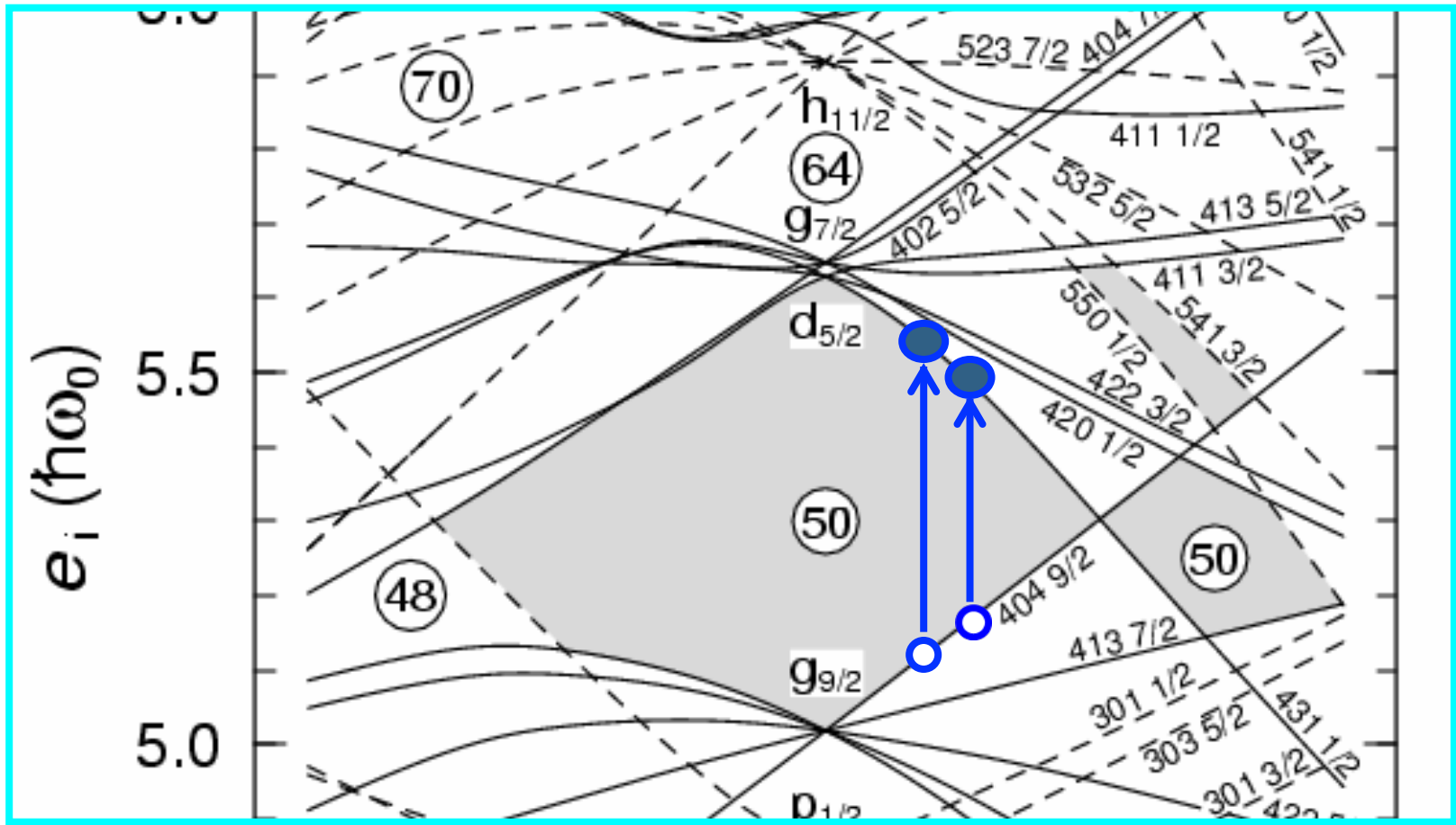
5. Most frequently the rotation takes place around the principal axis perpendicular to axis of symmetry



!!! Forbidden in quantum mechanics !!!



Maximum spin of the $N=50$ ground state is $I=0$

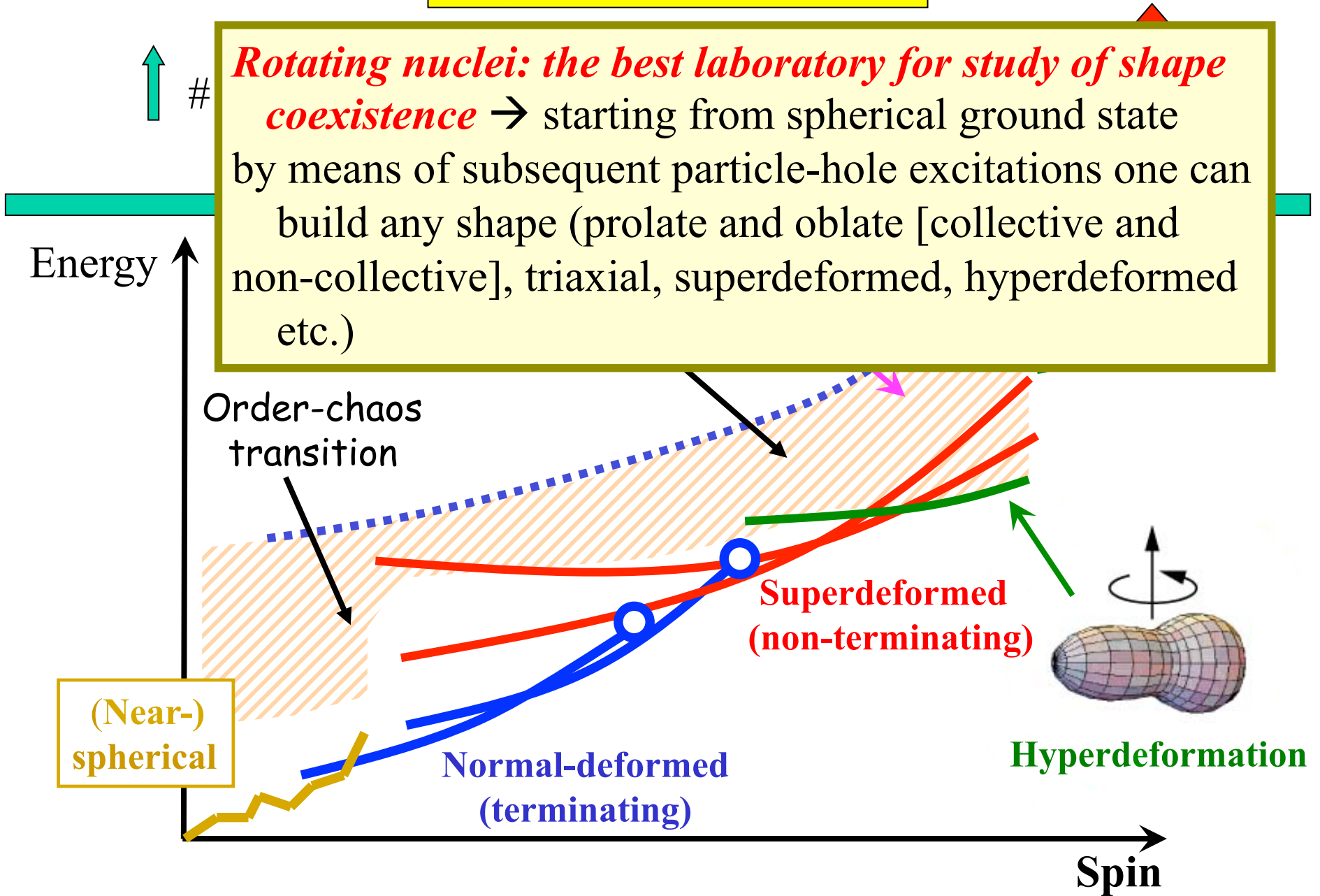


2p-2h excitation in the N=50 system → induces deformation
 → increases maximum spin in this configuration

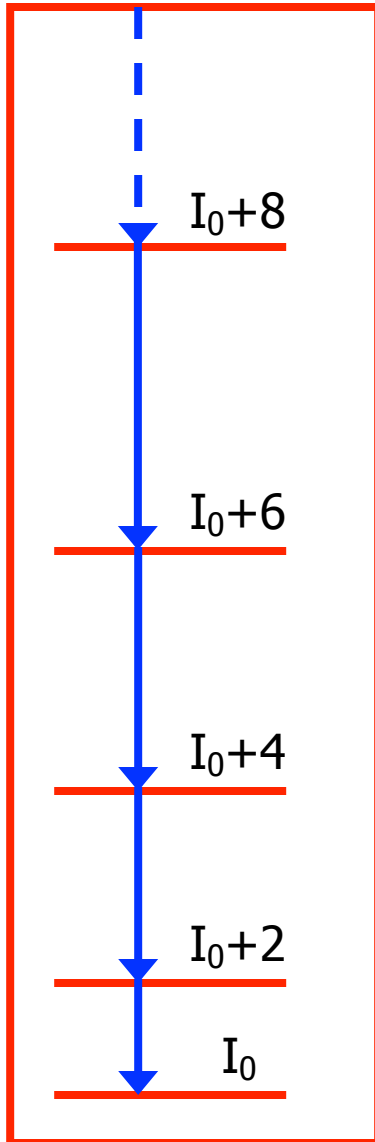
$$(g_{9/2})^{-2}_{4.5+3.5=8} (g_{7/2} d_{5/2})^2_{3.5+2.5=6} \Rightarrow I_{\max} = 14$$

High-spin laboratory

Rotating nuclei: the best laboratory for study of shape coexistence → starting from spherical ground state by means of subsequent particle-hole excitations one can build any shape (prolate and oblate [collective and non-collective], triaxial, superdeformed, hyperdeformed etc.)



Physical observables in rotating nuclei



Kinematic moment of inertia $J^{(1)}$

$$J_{band}^{(1)} = \frac{2I - 1}{E_{\gamma}(I \rightarrow (I - 2))} \text{ MeV}^{-1}$$

- inverse of the slope of the curve of energy E versus $I(I+1)$
- requires the knowledge of the spin

Dynamic moment of inertia $J^{(2)}$

$$J^{(2)}(I) = \frac{4}{E_{\gamma}((I + 2) \rightarrow I) - E_{\gamma}(I \rightarrow (I - 2))} \text{ MeV}^{-1}$$

- curvature of the of energy curve E versus $I(I+1)$
- Very useful for superdeformed bands which are not linked to the low-spin level scheme (spin I is not known)

Charge quadrupole moment

How to describe rotating nuclei ?

Rigid rotor: rotational excitation energies $E(I)$ obey the $I(I+1)$ rule'; I is spin

$$E(I) = \frac{\hbar^2}{2J} I(I+1)$$

J is moment of inertia

Transformation to rotating frame → CRANKING MODEL

$$\hat{H}^\omega = \hat{H} - \omega \hat{J}_x$$

Laboratory frame: potential V is time-dependent

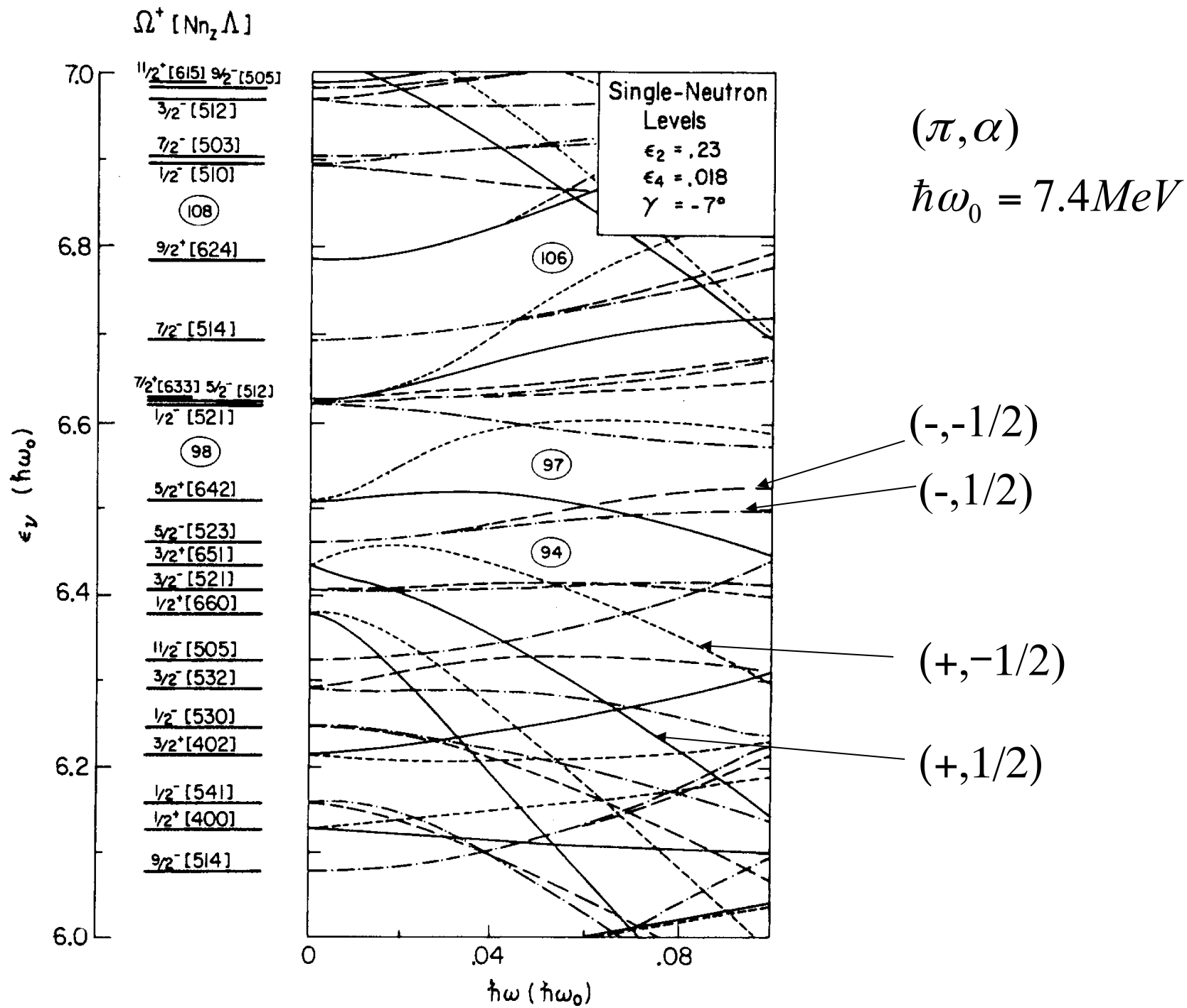
Rotating frame: potential V^* is time-independent

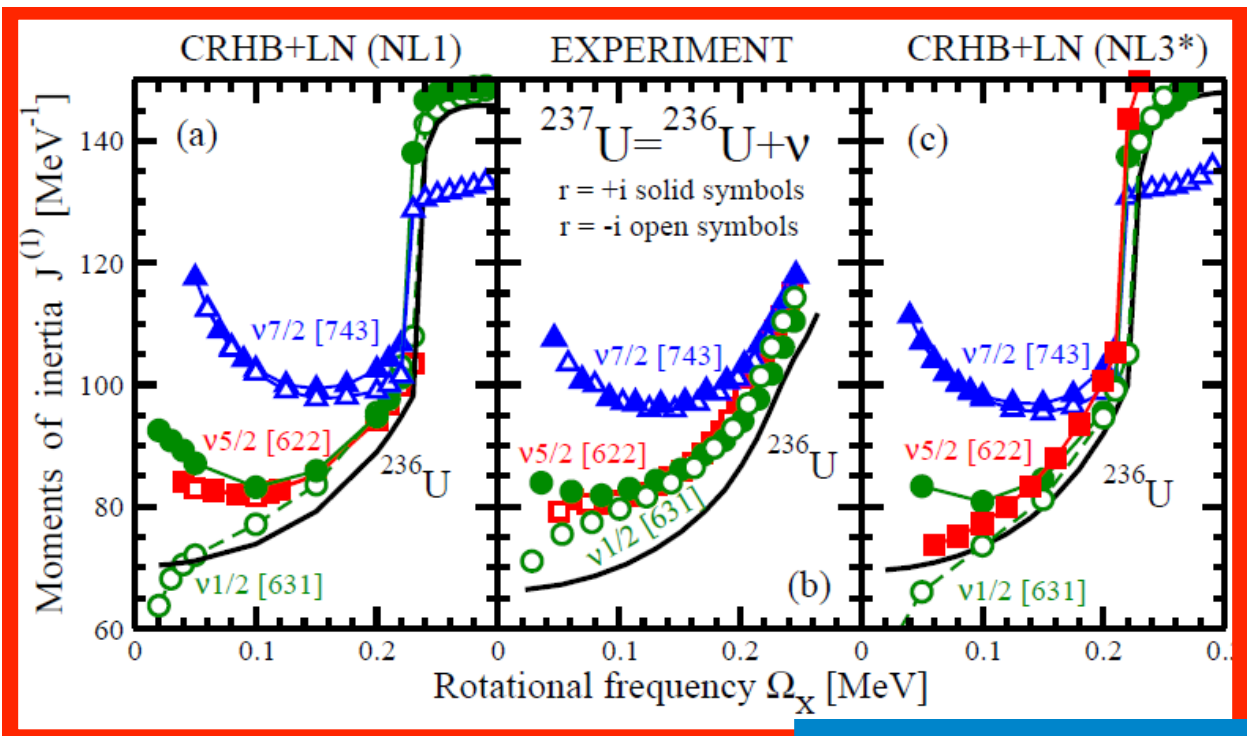
The state $|\rangle$ is the stationary mean field solution in the frame that rotates uniformly with the angular velocity ω about the x axis.

In the laboratory frame it corresponds to a uniformly rotating mean field state.

$$\langle | \hat{J}_x | \rangle = \sum_i \langle | \hat{j}_x | \rangle_i \quad \langle | \hat{J}_x | \rangle = \sqrt{I(I+1)}$$

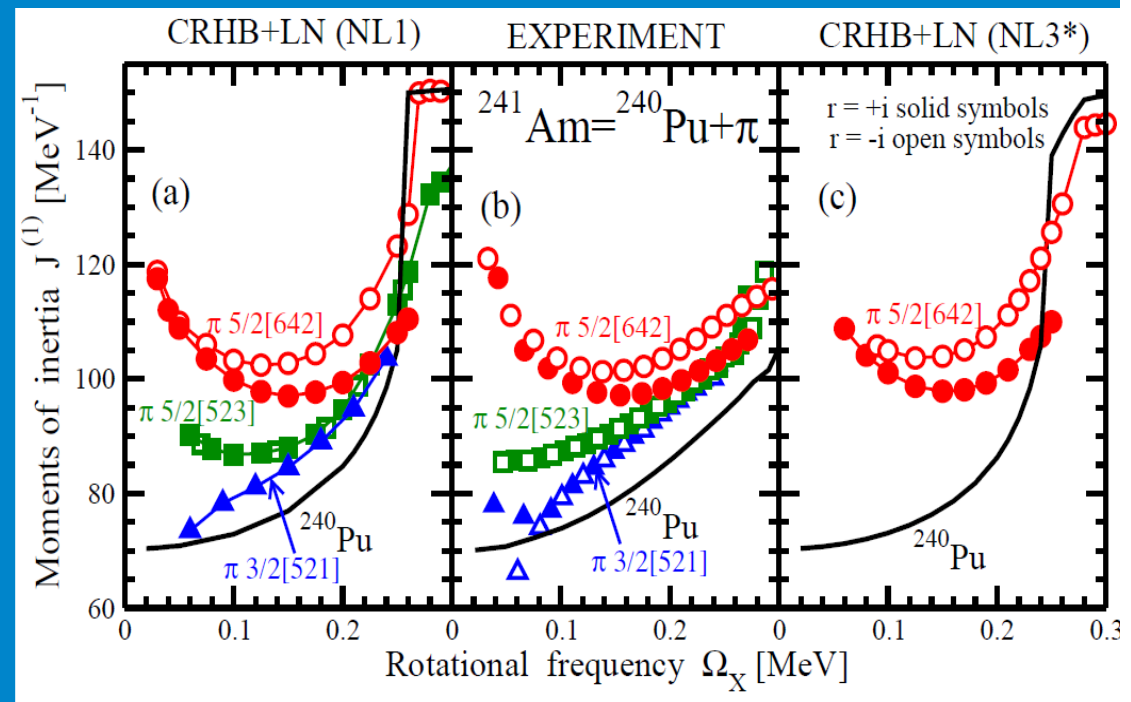
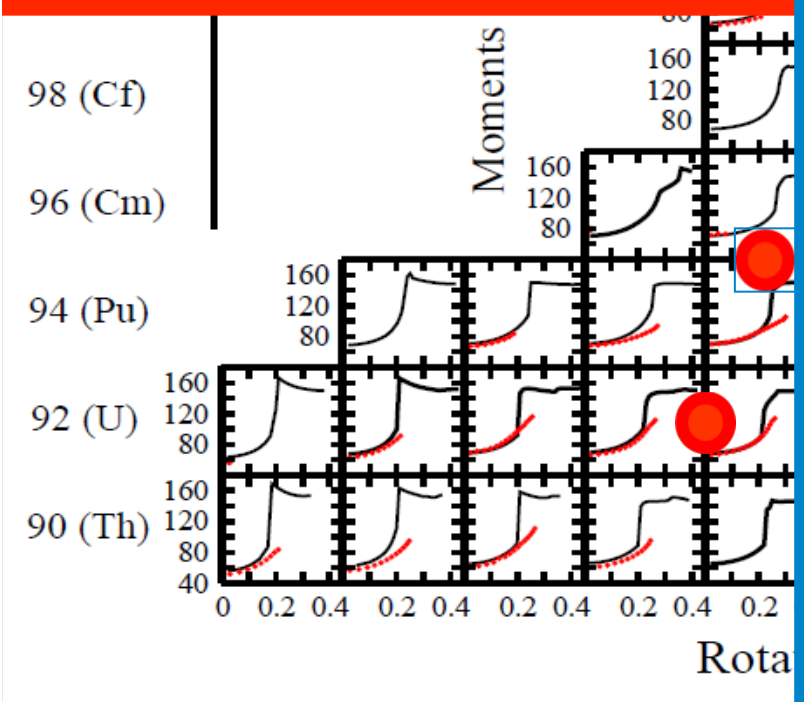
$$\begin{pmatrix} h_D - \lambda - \Omega_x \hat{J}_x & \hat{\Delta} \\ -\hat{\Delta}^* & -h_D^* + \lambda + \Omega_x \hat{J}_x \end{pmatrix} \begin{pmatrix} U_k \\ V_k \end{pmatrix} = E_k \begin{pmatrix} U_k \\ V_k \end{pmatrix}$$





Increase of $J^{(1)}$ in odd-proton nucleus as compared with even-even ^{240}Pu is due to blocking which includes:

- (a) Decrease of proton or neutron pairing
- (b) Alignment properties of blocked proton or neutron state

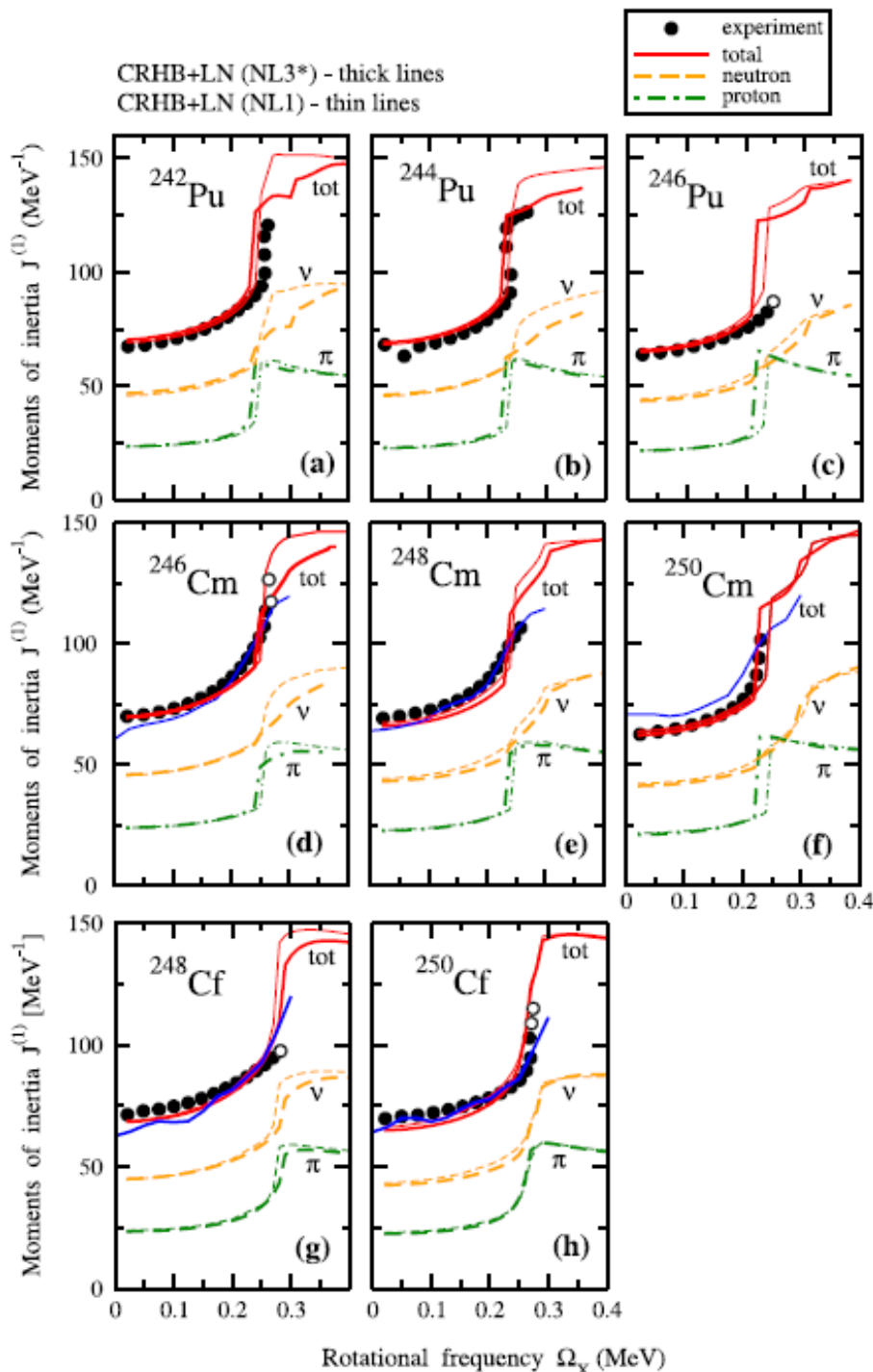


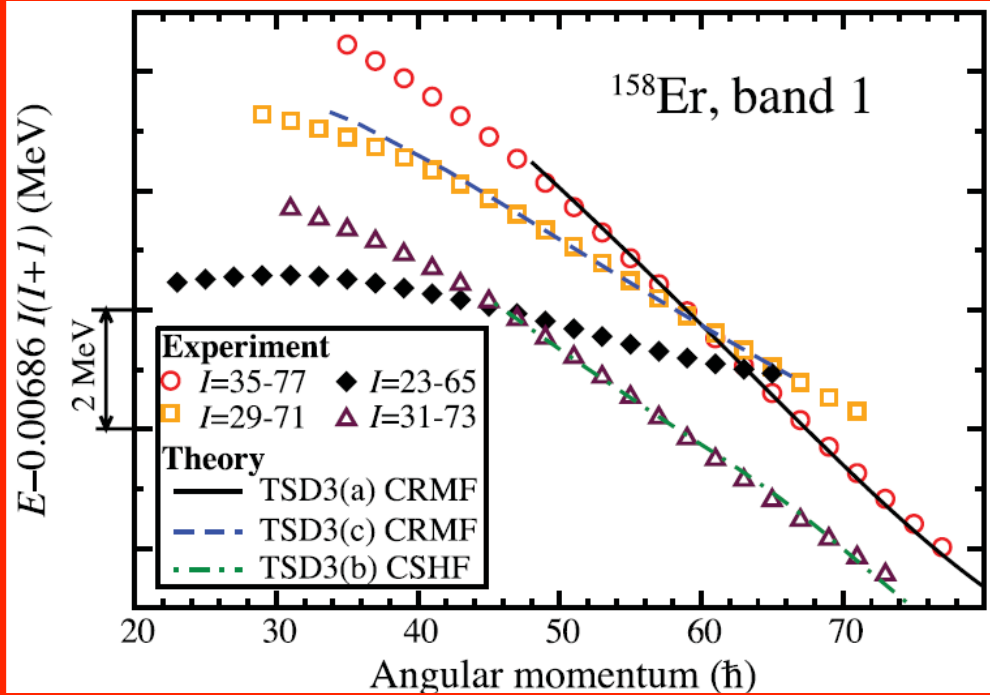
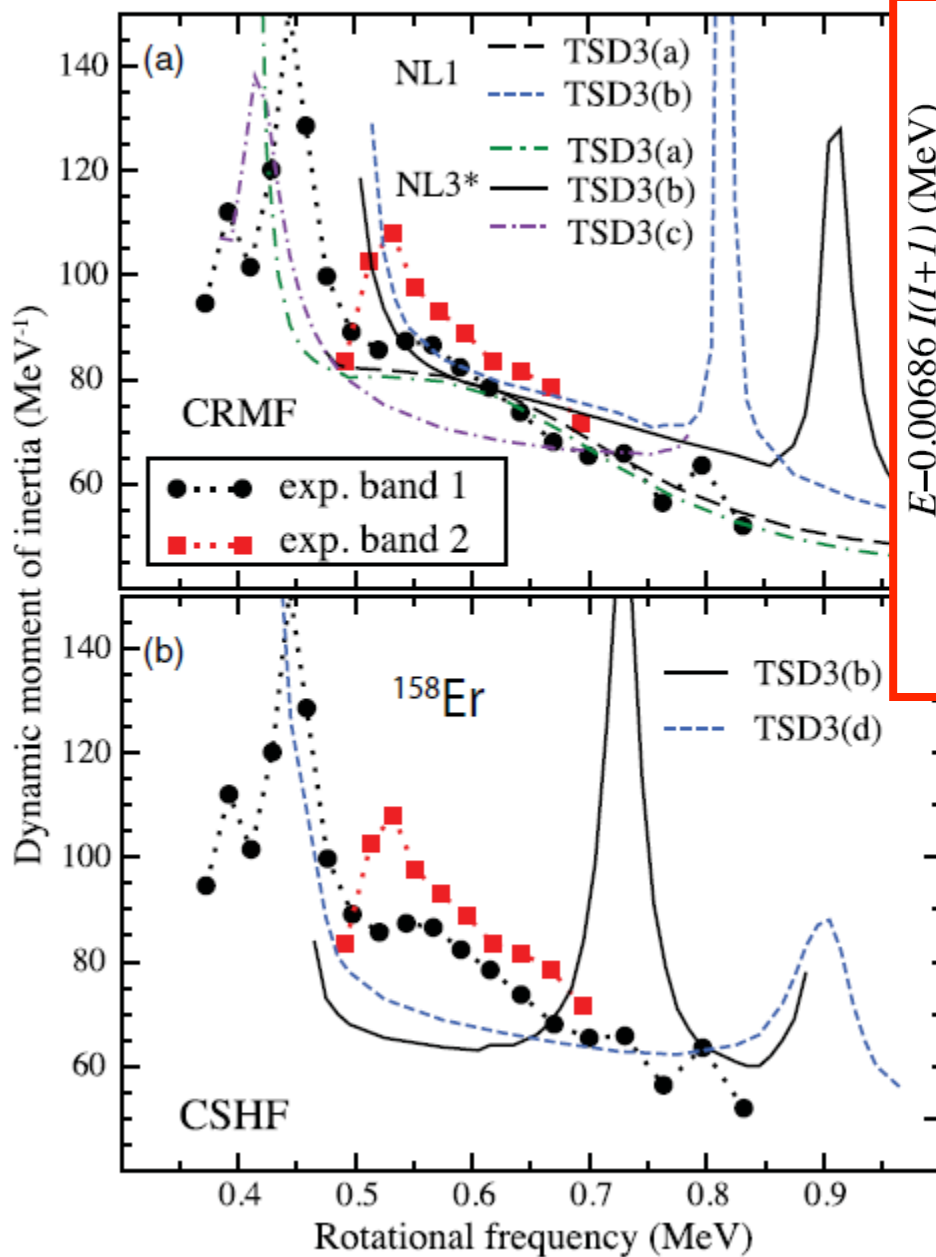
**Paired band crossings:
CRHB+LN versus
CSM+PNP**

CSM+PNP (Z.-H.Zhang et al, PRC 85, 014324 (2012)).

Carefull fit of:

- Parameters of Nilsson potential to the energies of the single-particle states
- Different pairing strength in even-even and odd nuclei
- Experimental deformations





DFT calculations suggest that band 1 in ^{158}Er is observed up to spin around 75

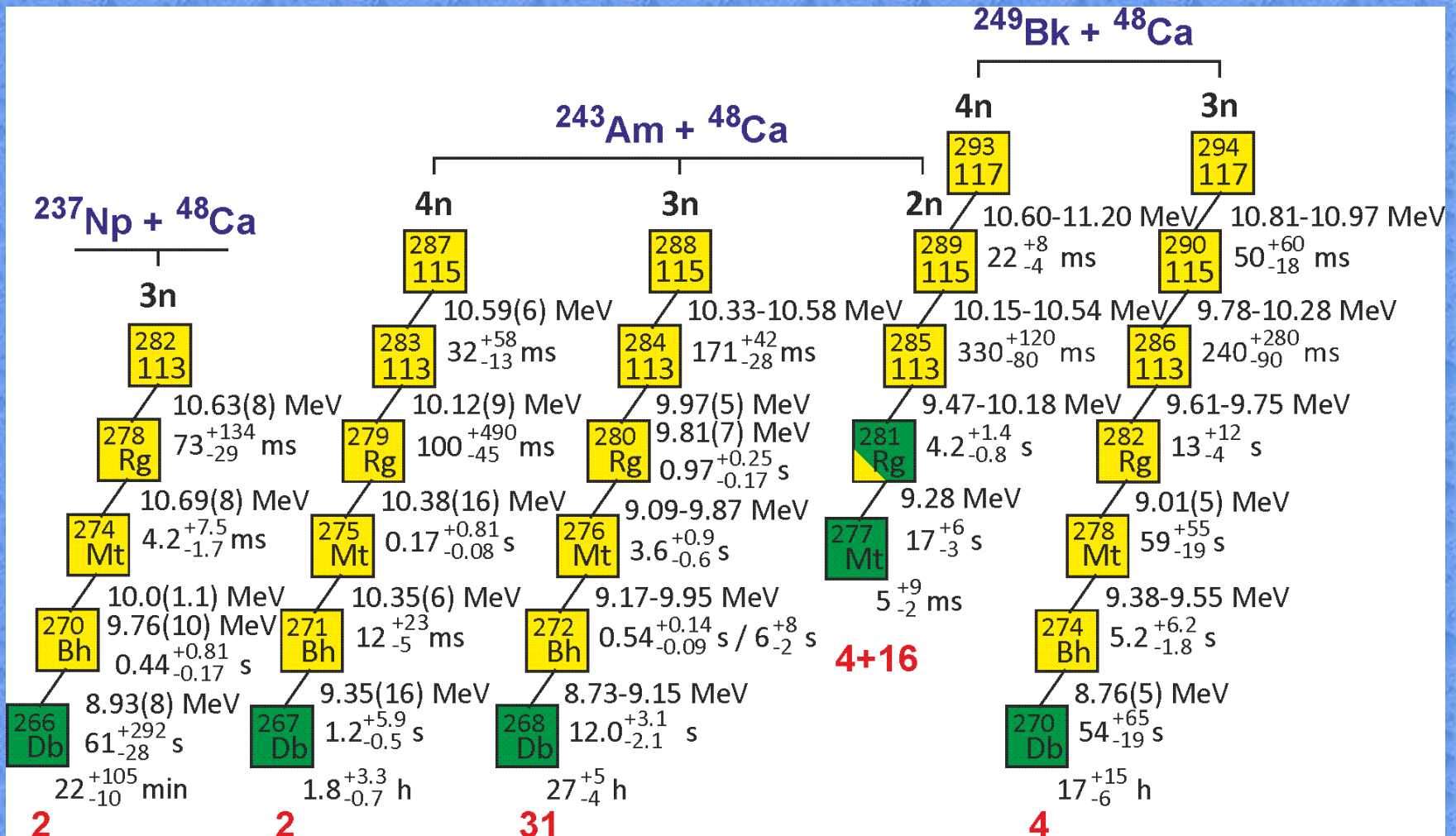
AA, Yue Shi, W.Nazarewicz,
PRC 86, 031304(R) (2012)

Nuclear structure: extras

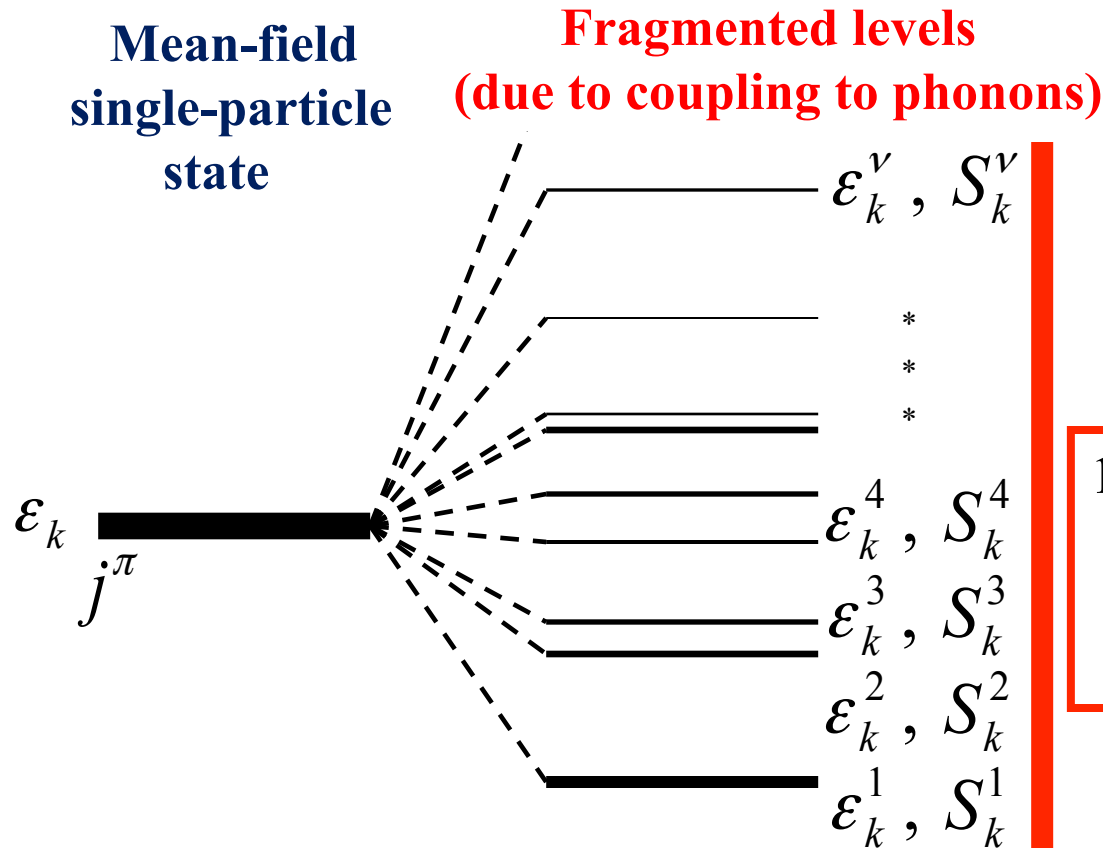
Anatoli Afanasjev
Mississippi State University

1. Nuclear theory – selection of starting point
2. What can be done 'exactly' (*ab-initio* calculations) and why we cannot do that systematically?
3. Effective interactions
4. Density functional theory
5. Shell structure and shell effects. Their consequences.
6. Nuclear landscape: what we know and how well we extrapolate
7. Superheavy nuclei: successes and challenges
8. Going beyond mean field: particle-vibration coupling in spherical nuclei
9. Going beyond mean field: gamma-soft nuclei
10. Rotating nuclei

What experimentalists see in experiment? α -decay chains



Can we obtain “bare” single-particle energies that can be used for comparison with plain DFT?



METHOD 1.

$$\varepsilon_k^{grav} = \left[\sum_{\nu} S_k^{\nu} \cdot \varepsilon_k^{\nu} \right] / \left[\sum_{\nu} S_k^{\nu} \right]$$

This energy is associated with a “bare” single-particle energy.

1. Spectroscopic factors depend on reaction and method of extraction:
example of spectroscopic factors in ^{209}Bi

| | | |
|--------------------|------|------|
| 1h _{9/2} | 1.17 | 0.80 |
| 2f _{7/2} | 0.78 | 0.76 |
| 1i _{13/2} | 0.56 | 0.74 |
| 2f _{5/2} | 0.88 | 0.57 |
| 3p _{3/2} | 0.67 | 0.44 |
| 3p _{1/2} | 0.49 | 0.20 |

($^3\text{He},d$) (α,t) reactions

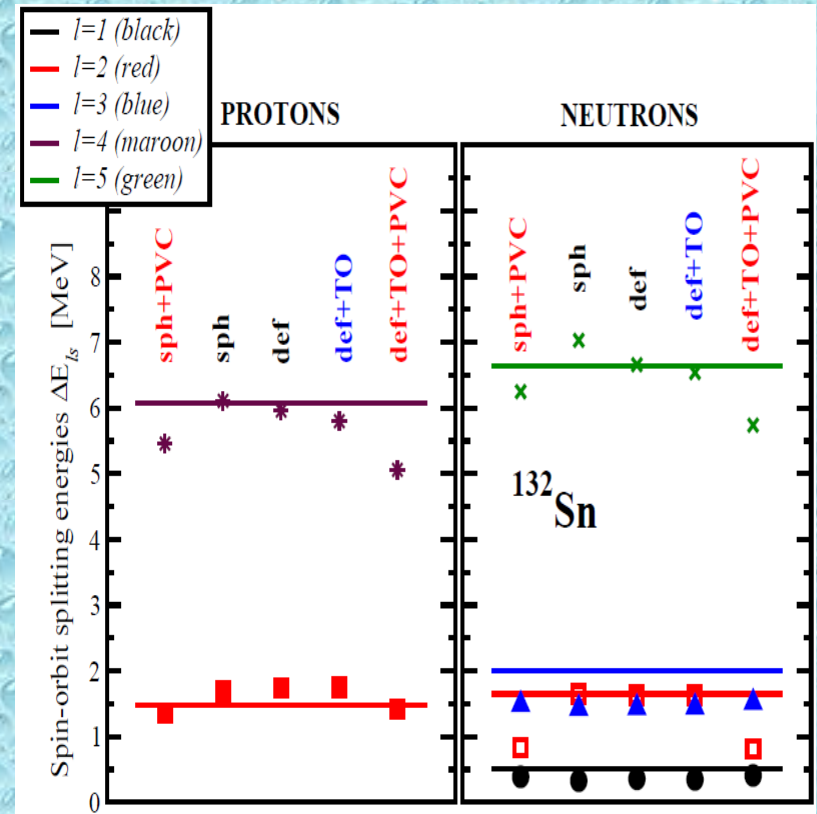
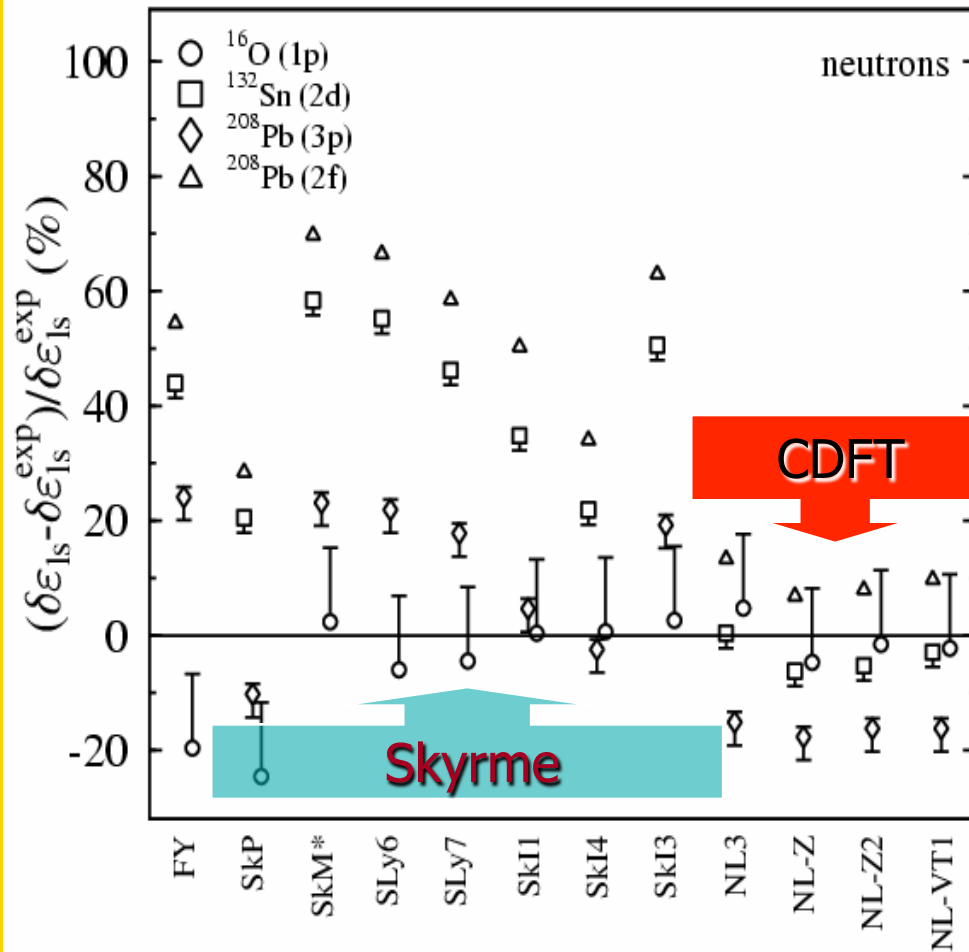
2. Spins and parities of fragments are frequently not measured.
3. Some fragments are not observed.
4. Sum rule $\sum_{\nu} S_k^{\nu} = 1$ is frequently violated.

Spin-orbit splitting

Spin – orbit interaction – fully relativistic phenomenon

PVC; E.V. Litvinova and AA, PRC 84, 014305 (2011)

Mean field level;
M.Bender et al, PRC 60 (1999) 034304



The absolute deviations per doublet are **0.34 MeV [0.50 MeV]**, **0.23 MeV [0.56 MeV]** and **0.26 MeV [0.45 MeV]** in the mean field (“def+TO”) [**particle-vibration coupling** (“def+TO+PVC”)] calculations in ^{56}Ni , ^{132}Sn and ^{208}Pb , respectively.

Spectroscopic factors

The absolute values of experimental spectroscopic factors are characterized by large ambiguities and depend strongly on the reaction employed in experiment and the reaction model used in the analysis

| Nucleus | State | S_{th} | S_{exp} | S_{exp} |
|-------------------|-------------|----------|---------------------|-------------|
| ^{209}Pb | $2g_{9/2}$ | 0.85 | 0.78 ± 0.1 [76] | 0.94 [80] |
| | $1i_{11/2}$ | 0.89 | 0.96 ± 0.2 [76] | 1.05 [80] |
| | $1j_{15/2}$ | 0.66 | 0.53 ± 0.2 [76] | 0.57 [80] |
| | $3d_{5/2}$ | 0.89 | 0.88 ± 0.1 [76] | |
| | $4s_{1/2}$ | 0.92 | 0.88 ± 0.1 [76] | |
| | $2g_{7/2}$ | 0.87 | 0.78 ± 0.1 [76] | |
| | $3d_{3/2}$ | 0.89 | 0.88 ± 0.1 [76] | |
| ^{209}Bi | $1h_{9/2}$ | 0.88 | 1.17 [75] | 0.80 [69] |
| | $2f_{7/2}$ | 0.78 | 0.78 [75] | 0.76 [69] |
| | $1i_{13/2}$ | 0.63 | 0.56 [75] | 0.74 [69] |
| | $2f_{5/2}$ | 0.61 | 0.88 [75] | 0.57 [69] |
| | $3p_{3/2}$ | 0.62 | 0.67 [75] | 0.44 [69] |
| | $3p_{1/2}$ | 0.37 | 0.49 [75] | 0.20 [69] |
| ^{207}Pb | $3p_{1/2}$ | 0.90 | | 1.08 [83] |
| | $2f_{5/2}$ | 0.87 | 1.13 [78] | 1.05 [83] |
| | $3p_{3/2}$ | 0.86 | 1.00 [78] | 0.95 [83] |
| | $1i_{13/2}$ | 0.82 | 1.04 [78] | 0.61 [83] |
| | $2f_{7/2}$ | 0.64 | 0.89 [78] | 0.64 [83] |
| | $1h_{9/2}$ | 0.38 | | |
| ^{207}Tl | $3s_{1/2}$ | 0.84 | 0.95 [77] | 0.85 [68] |
| | $2d_{3/2}$ | 0.86 | 1.15 [77] | 0.90 [68] |
| | $1h_{11/2}$ | 0.80 | 0.89 [77] | 0.88 [68] |
| | $2d_{5/2}$ | 0.68 | 0.62 [77] | 0.63 [68] |
| | $1g_{7/2}$ | 0.22 | 0.40 [77] | 0.27 [68] |

| Nucleus | State | S_{th} | S_{exp} [79] | S_{exp} [59] |
|------------------|------------|----------|-----------------|-----------------|
| ^{57}Ni | $2p_{3/2}$ | 0.83 | 0.95 ± 0.29 | 0.58 ± 0.11 |
| | $1f_{5/2}$ | 0.79 | 1.40 ± 0.42 | |
| | $2p_{1/2}$ | 0.76 | 1.00 ± 0.30 | |
| | $1g_{9/2}$ | 0.79 | | |

| Nucleus | State | S_{th} | S_{exp} |
|-------------------|------------|----------|-----------------|
| ^{133}Sn | $2f_{7/2}$ | 0.89 | 0.86 ± 0.16 |
| | $3p_{3/2}$ | 0.91 | 0.92 ± 0.18 |
| | $1h_{9/2}$ | 0.88 | |
| | $3p_{1/2}$ | 0.91 | 1.1 ± 0.3 |
| | $2f_{5/2}$ | 0.89 | 1.1 ± 0.2 |